Electronic Supplementary Material (ESI) for Chemical Science.


# EXPERIMENTAL SECTION

## Development of $^{68}$Ga-labelled Ultrasound Microbubbles for Whole-body PET Imaging

Javier Hernández-Gil,*[a] Marta Braga,[b] Bethany I. Harriss,[a] Laurence S. Carroll, [b] Chee Hau Leow,[c] Meng-Xing Tang,[c] Eric O. Aboagye,*[b] and Nicholas J. Long*[a]

## Lipid formulations:

**Table S1**. Formulation of unmodified MBs.

| Lipid | Mw ($g \cdot mol^{-1}$) | Mass (mg) | Mol (µmol) | Mol ratio (%) |
|---|---|---|---|---|
| DPPC | 734.04 | 0.660 | 0.899 | 85 |
| LPC | 495.63 | 0.050 | 0.101 | 10 |
| DSPE-PEG2000-$NH_2$ | 2790.49 | 0.150 | 0.054 | 5 |

**Table S2**. Formulation of MBs containing 10 % PE phospholipid.

| Lipid | Mw ($g \cdot mol^{-1}$) | Mass (mg) | Mol (µmol) | Mol ratio (%) |
|---|---|---|---|---|
| DPPC | 734.04 | 0.650 | 0.886 | 85 |
| PE | 748.07 | 0.080 | 0.107 | 10 |
| DSPE-PEG2000-$NH_2$ | 2790.49 | 0.140 | 0.050 | 5 |

**Table S3**. Formulation of MBs containing 10 % PE-$PEG_4$-TCO phospholipid.

| Lipid | Mw ($g \cdot mol^{-1}$) | Mass (mg) | Mol (µmol) | Mol ratio (%) |
|---|---|---|---|---|
| DPPC | 734.04 | 0.620 | 0.845 | 85 |
| PE-$PEG_4$-TCO | 1147.80 | 0.120 | 0.105 | 10 |
| DSPE-PEG2000-$NH_2$ | 2790.49 | 0.140 | 0.050 | 5 |

**Table S4.** Comparison of the different MB formulations (replicates = 4-6).

| | **Unmodified** | **10% PE** | **10% PE-PEG$_4$-TCO** |
|---|---|---|---|
| **Concentration (MB/mL)[a]** | $(8.02 \pm 0.03)\cdot10^9$ | $(1.22 \pm 0.68)\cdot10^{10}$ | $(1.57 \pm 0.34)\cdot10^{10}$ |
| **Mean Diameter (µm)[a]** | 2.18 ± 1.06 | 2.10 ± 1.07 | 2.40 ± 1.33 |
| **Range (µm)[a]** | 0.53 – 8.96 | 0.52 – 9.80 | 0.51 – 9.90 |
| **ζ-potential (mV)[b]** | 14.4 ± 1.6 | 11.1 ± 1.1 | 12.4 ± 1.1 |
| **MB contrast (a.u.)[c]** | 536.9 ± 29.7 | 545.5 ± 89.4 | 540.3 ± 57.0 |

[a] MBs were sized and counted using a bright-field microscope (Nikon Eclipse 50i, 40× objective) and according to a standard protocol in or group[2]; [b] a 1:100 diluted sample in PBS was used for ζ-potential measurements using a Malvern Nano ZetaSizer; [c] the ultrasound contrast enhancement was quantified using a custom designed 'imaging-activation-imaging' sequence on a Verasonics Vantage 256 research platform. Single cycle, low amplitude ultrasound at 4.5 MHz (number of half cycle = 1, Number of angle compounding = 15, Number of frames per time = 10).) was used at each imaging step to estimate the ultrasound signal level from the contrast agent. The same amount of stock MBs was introduced into a 2L water tank filled with water and equilibrated to 37°C to achieve a final concentration of approximately $10^6$ MBs/mL. Before each acquisition, the water was mixed to achieve a relatively uniform distribution of droplets. Acoustic absorbers were used to line the water tank to reduce ultrasound reflections (S. Li, S. Lin, Y. Cheng, T. O. Matsunaga, R. J. Eckersley, M.-X. Tang, *Ultrasound Med. Biol.* **2015**, *41*, 1422-1431; b) H. Mulvana, E. Stride, M-X. Tang, J. V. Hajnal, R. J. Eckersley, *Ultrasound Med. Biol.* **2012**, *38*, 1097-1100).

**Table S5**. Summary of different cartridges used for lipid purification.

| Cartridge Type | Initial activity (%) | Activity trapped (%) | Activity eluted (%) | Activity left in cartridge (%) |
|---|---|---|---|---|
| Oasis® Prime [a] | 100 | 66 ± 10 | 0 | 62 ± 15 |
| Oasis® HLB [b] | 100 | 46 ± 8 | 27 ± 5 | 17 ± 3 |
| HybridSPE® [c] | 100 | 47 ± 9 | 15 ± 5 | 32 ± 7 |

[a] Cartridge not activated, washing: $H_2O$, elution: pure EtOH.

[b] Activation: 10 mL EtOH + 10 mL $H_2O$, washing: $H_2O$, elution: pure EtOH.

[c] Cartridge not activated, washing: $H_2O$, elution: 5% $NH_4OH$ in EtOH.

Different solid-phase extraction (SPE) cartridges were tested for [$^{68}$Ga][Ga(**1**)] purification, but unfortunately all sorbents presented low recovery yields (Table S1), observing a considerable amount of activity (60-20% of initial activity) retained in the different cartridges.

In addition to above sorbents, reverse-phase silica sorbents (i.e. C4, C8, and tC18) were used, but the trapping of [$^{68}$Ga][Ga(**1**)] was lower than 10-20% in all cases.

## Radiochromatograms of [$^{68}$Ga][Ga(5)] labelling

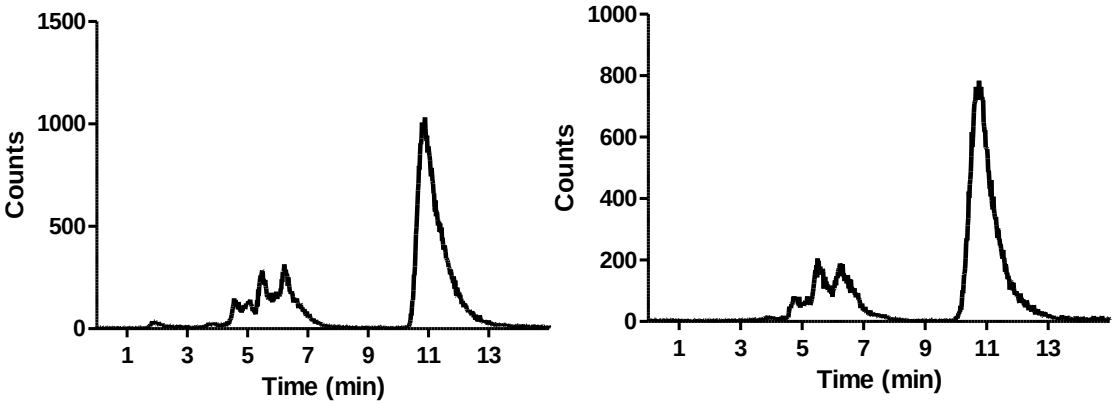


**Figure S1.** Radio-HPLC profile of labelled HBED-CC-Tetrazine (**5**) at 90 ºC (left) and, at room temperature (right) for 10 min.

## Radiochromatograms monitoring the reaction between PE-PEG$_4$-TCO (4) and [$^{68}$Ga][Ga(5)] or [$^{68}$Ga][Ga(6)]

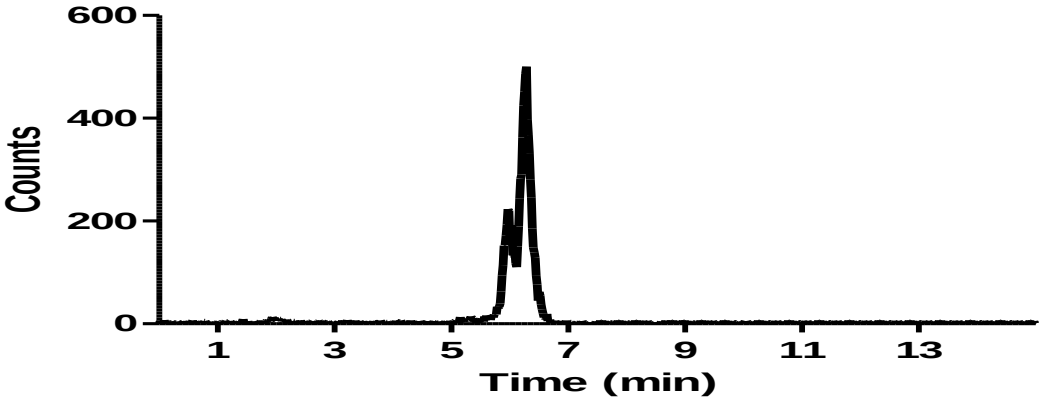


**Figure S2.** Radio-HPLC profile of labelled DOTA-GA-Tetrazine (**6**) and PE-PEG$_4$-TCO (**4**) in neutral conditions: (left) after 1 min and, (right) after 20 min at 60 ºC (mobile phase: 100 mM ammonium formate/methanol).

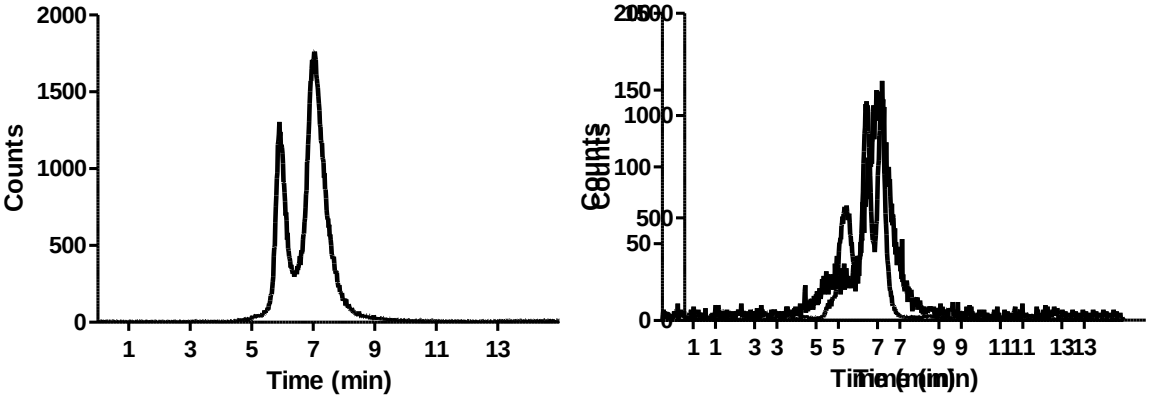


**Figure S3.** Two typical examples showing radio-HPLC profiles of labelled HBED-CC-Tetrazine (**5**) and PE-PEG$_4$-TCO (**4**) reaction after 20 min at 60 ºC (mobile phase: 100 mM ammonium formate/methanol).

**Radiochromatogram of the first wash after centrifuging $^{68}$Ga-labelled MBs:**

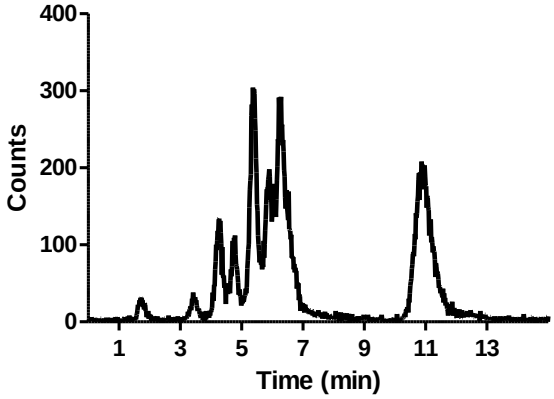


**Figure S4.** Radio-HPLC profile of infranatant after MB purification by centrifugation showing unreacted HBED-CC-Tetrazine (**5**) and free reacted lipid $^{68}$Ga-HBED-CC-PE.

## In vivo results

### Tissue kinetics and biodistribution of [$^{68}$Ga][Ga(5)]

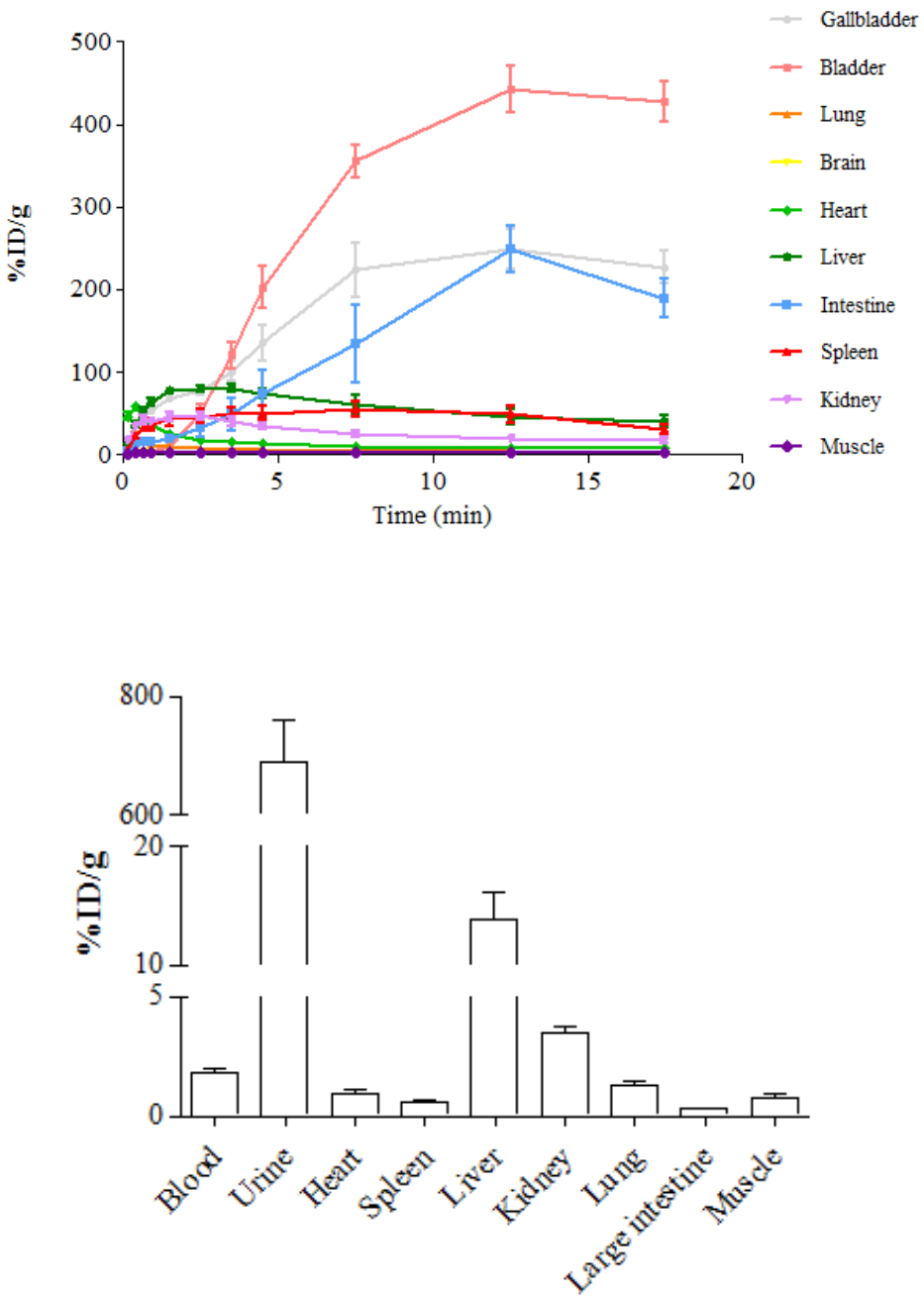


**Figure S5.** (top) Time activity curves following the injection of [$^{68}$Ga][Ga(**5**)] and, (bottom) tissue biodistribution of [$^{68}$Ga][Ga(**5**)] at 20 min post-injection in Balb/c nude mice (n = 5).

**Tissue kinetics and biodistribution of $^{68}$Ga-labelled-PE phospholipid**

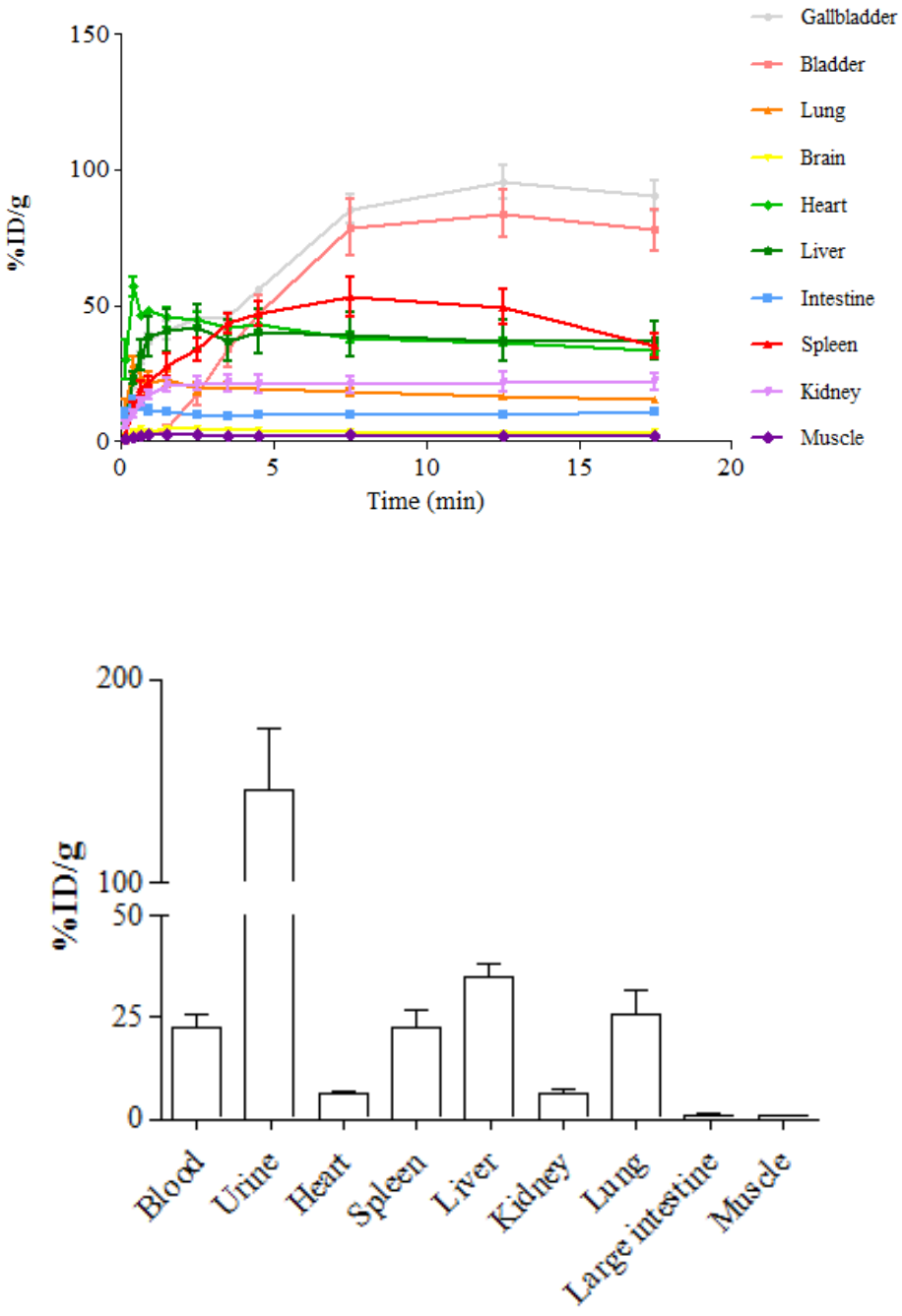


**Figure S6.** (top) Time activity curves following the injection of $^{68}$Ga-labelled PE phospholipid and, (bottom) tissue biodistribution of $^{68}$Ga-labelled PE phospholipid at 20 min post-injection in Balb/c nude mice (n = 5).

## Tissue kinetics and biodistribution of $^{68}$Ga-labelled MBs

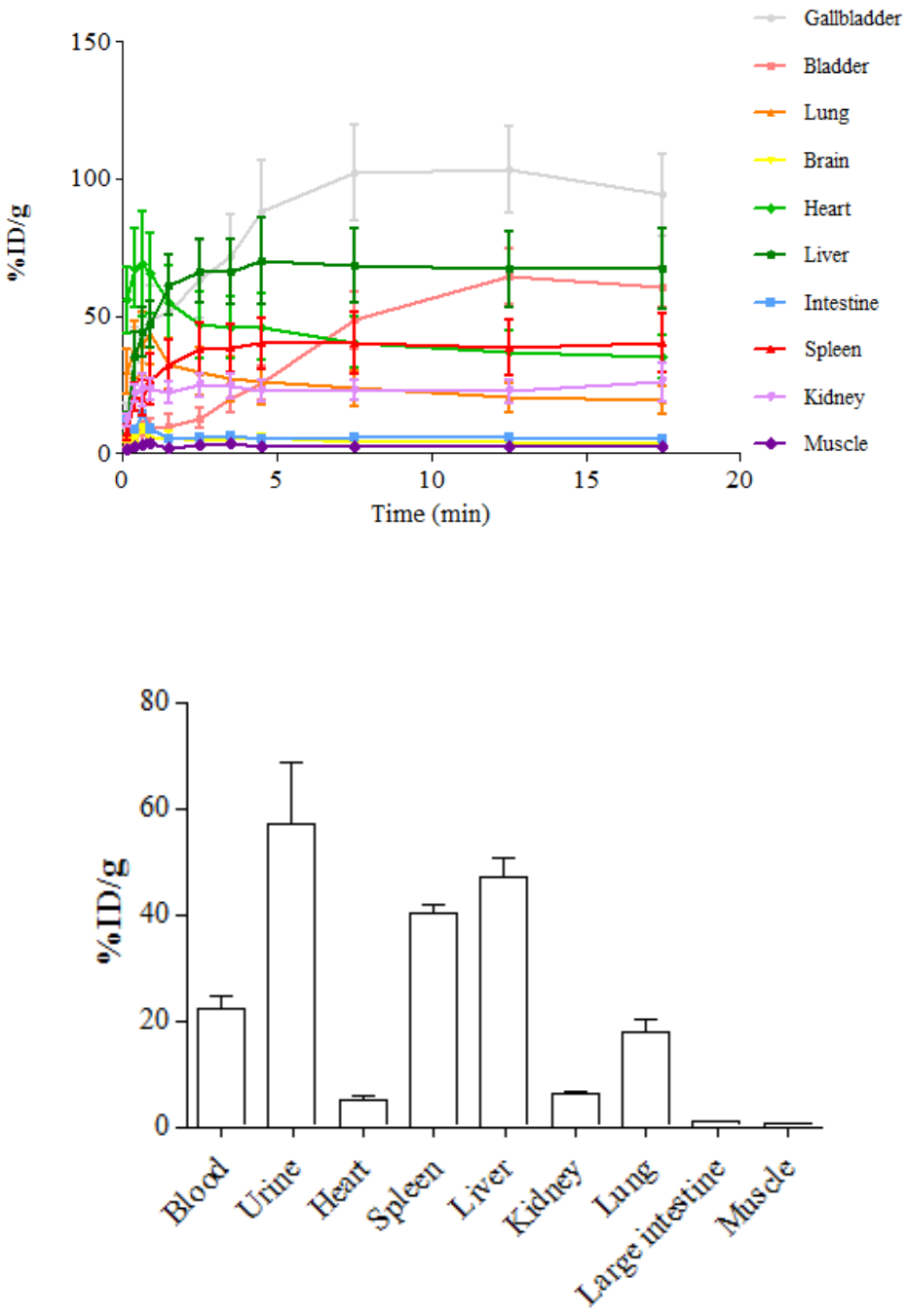


**Figure S7.** (top) Time activity curves following the injection of $^{68}$Ga-labelled MBs and, (bottom) tissue biodistribution of $^{68}$Ga-labelled MBs at 20 min post-injection in Balb/c nude mice (n = 6).

# 7. NMR AND MS SPECTRA

## Characterization of PE-NOTA (1)

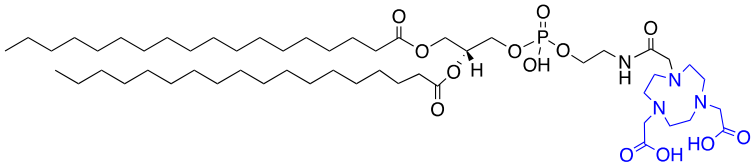

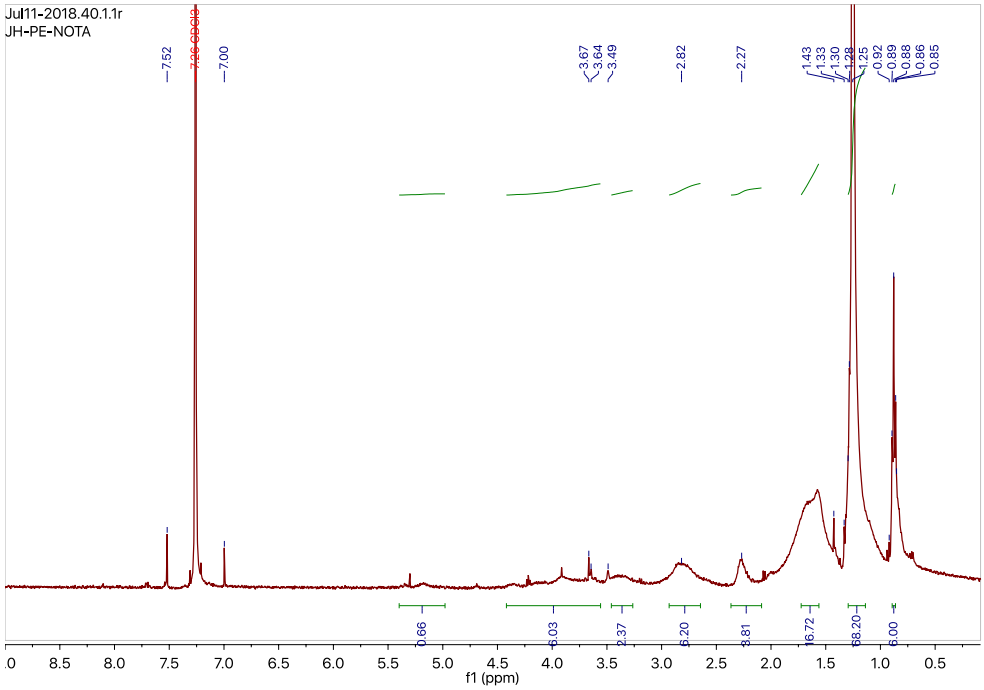


**Figure S8.** $^{1}H$ NMR spectrum of PE- NOTA (**1**) in $CDCl_3$.

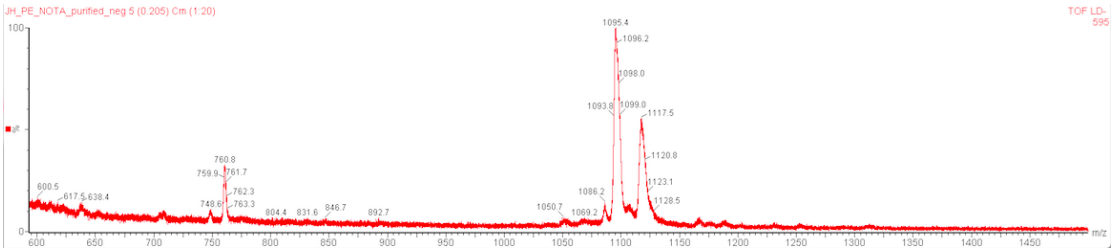


**Figure S9.** MALDI-TOF spectrum of PE-NOTA (**1**).

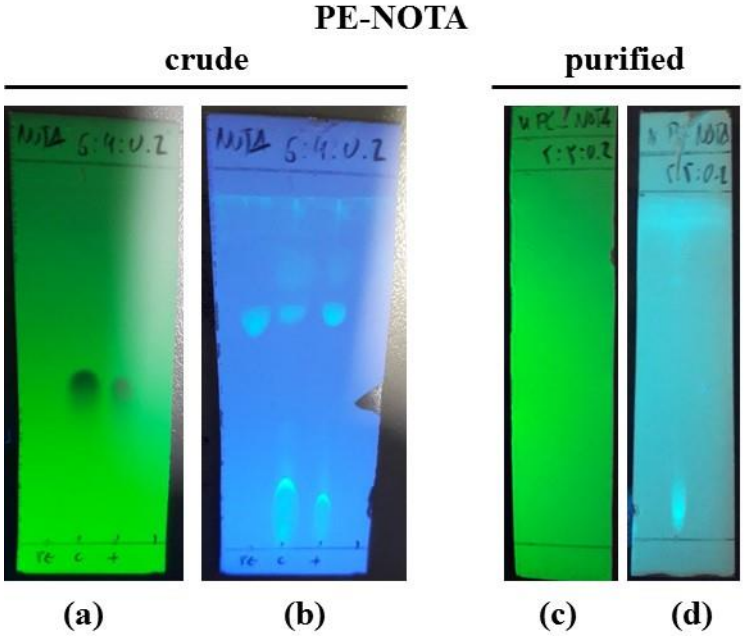


**Figure S10.** TLC plates of PE-NOTA reaction and purified lipid. (a) and (c) under 254 nm UV lamp and, (b) and (d) under 365 nm UV lamp and stained with a solution of 5% primuline. Mobile phase used for all plates composed of $CHCl_3$:MeOH:$H_2O$: a and b (6:4:0.2), c and d (5:5:0.2). PE = PE-$NH_2$ lipid, C = crude and, + = co-spot.

## Characterization of PE-DOTA (2)

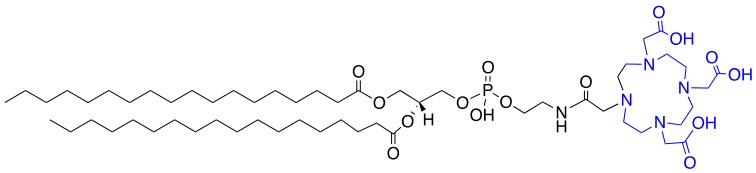

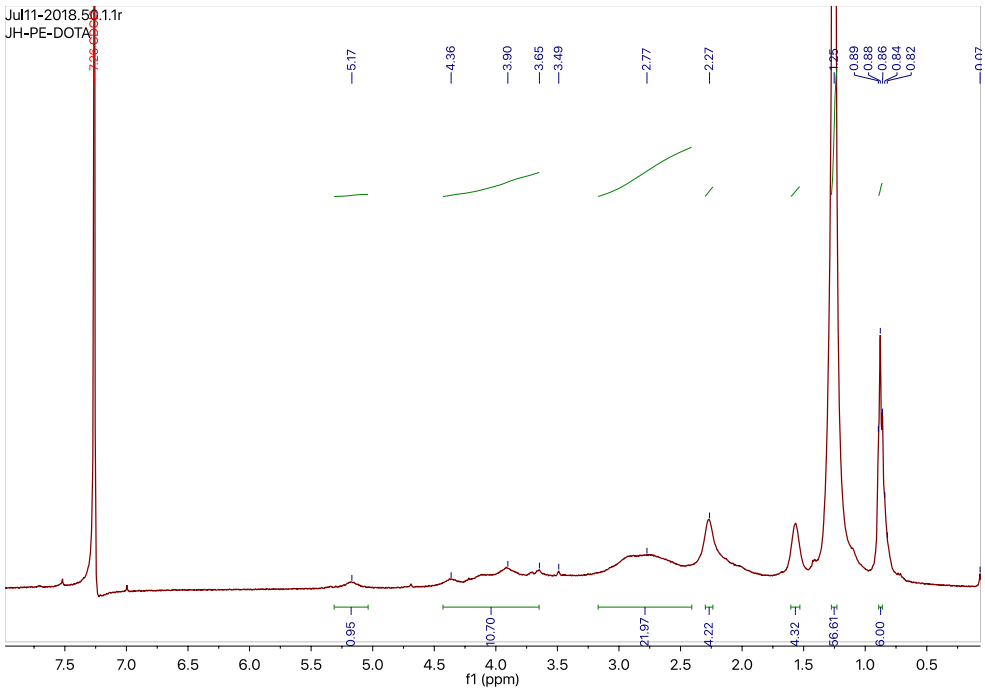


**Figure S11.** $^{1}$H NMR spectrum of PE-DOTA (**2**) in $CDCl_3$.

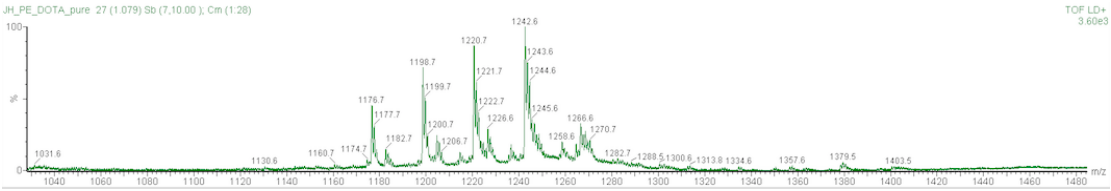


**Figure S12.** MALDI-TOF spectrum of PE-DOTA (**2**).

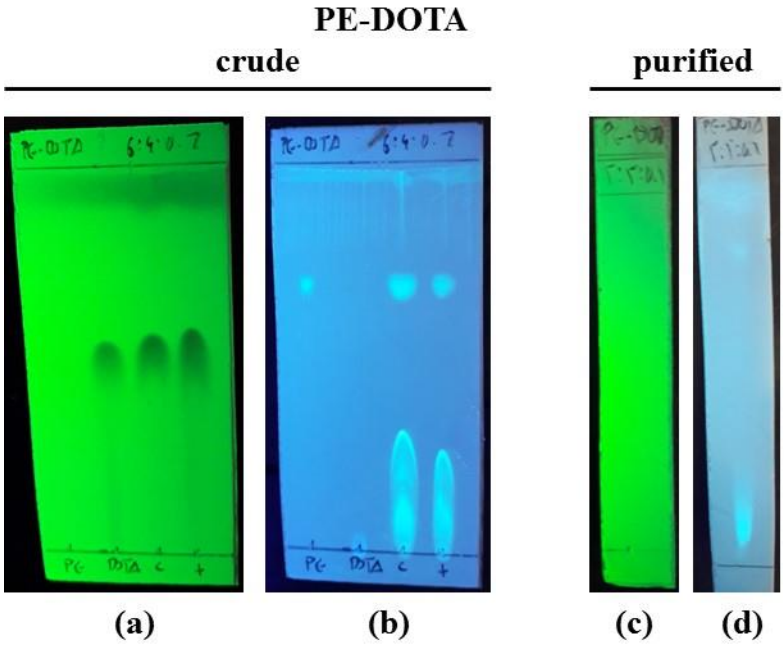


**Figure S13.** TLC plates of PE-DOTA reaction and purified lipid. (a) and (c) under 254 nm UV lamp and, (b) and (d) under 365 nm UV lamp and stained with a solution of 5% primuline. Mobile phase used for all plates composed of $CHCl_3$:MeOH:$H_2O$: a and b (6:4:0.2), c and d (5:5:0.2). PE = PE-$NH_2$ lipid, DOTA = DOTA- NHS, C = crude and, + = co-spot.

## Characterization of PE-isothiocyanate

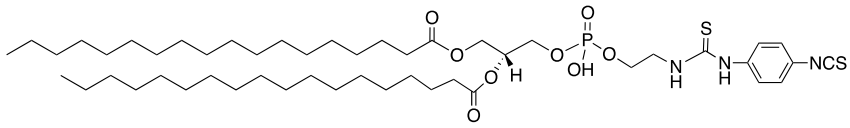


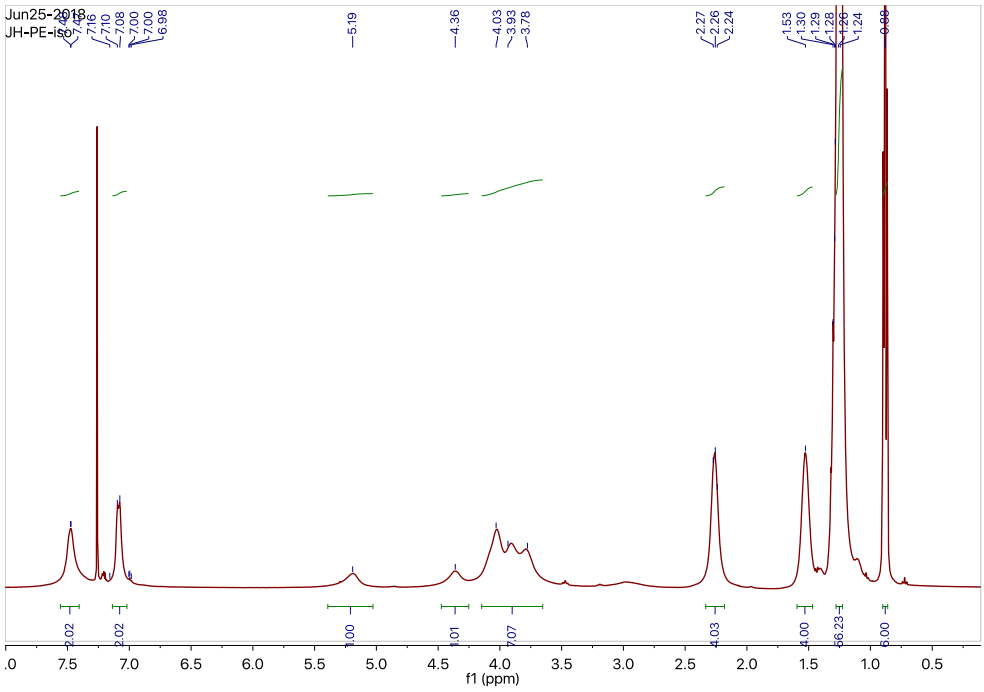


**Figure S14.** $^{1}H$ NMR spectrum of PE-isothiocyanate in $CDCl_3$.

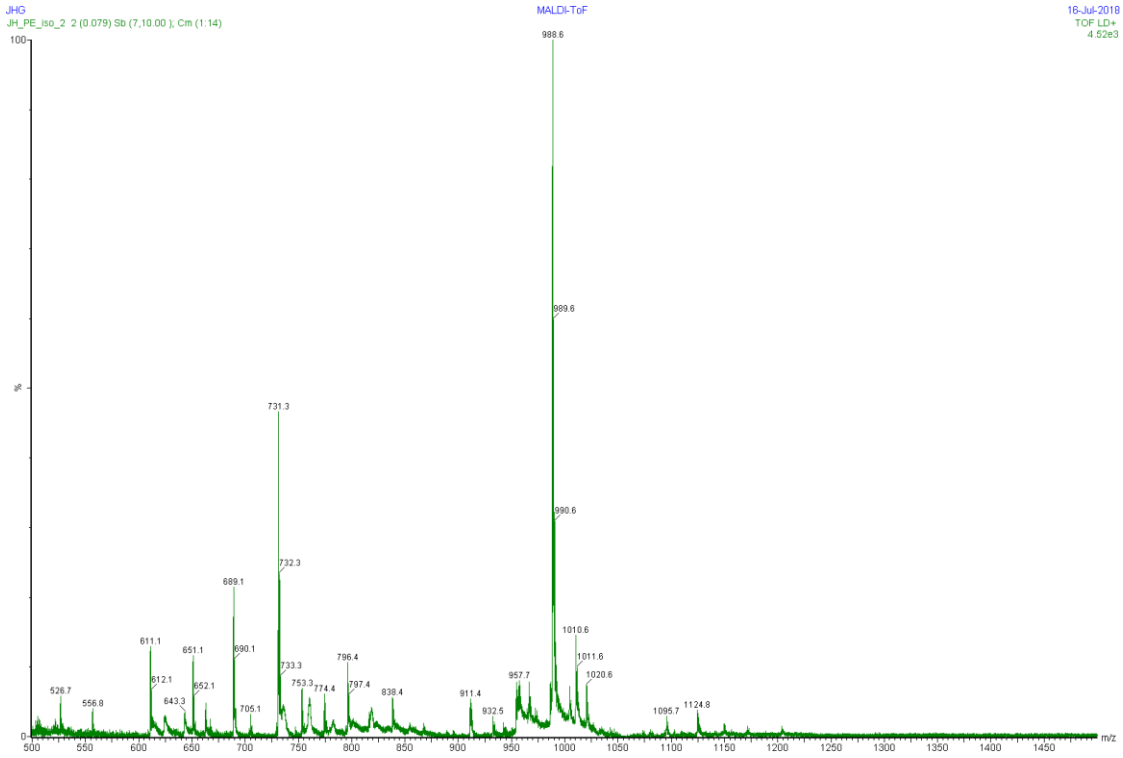


**Figure S15.** MALDI-TOF spectrum of PE-isothiocyanate.

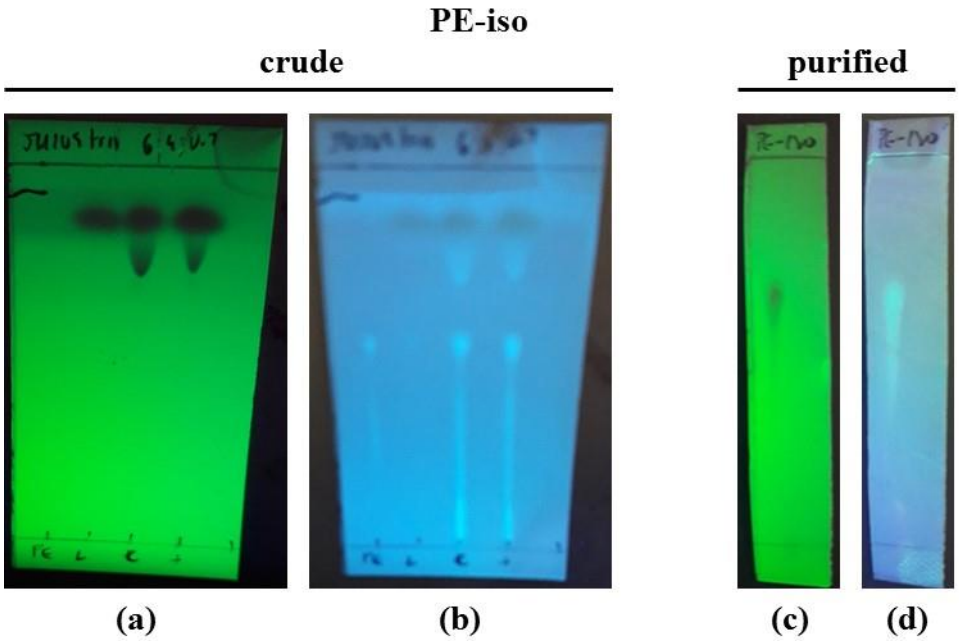


**Figure S16.** TLC plates of PE-iso reaction. (a) and (c) under 254 nm UV lamp and, (b) and (d) under 365 nm UV lamp and stained with a solution of 5% primuline. Mobile phase used for both plates composed of $CHCl_3$:MeOH:$H_2O$: a and b (6:4:0.2) and, c and d plate (9:1:0.2). PE = PE-$NH_2$ lipid, L = *p*-phenylene diisothiocyanate, C = crude and, + = co-spot.

## Characterization of PE-iso-DOTA-GA (3)

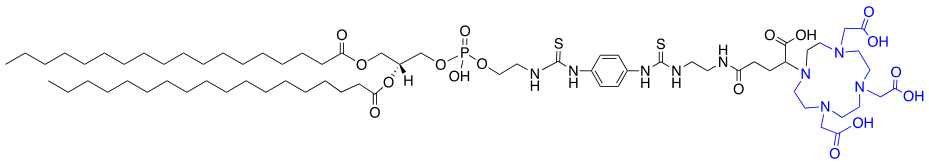

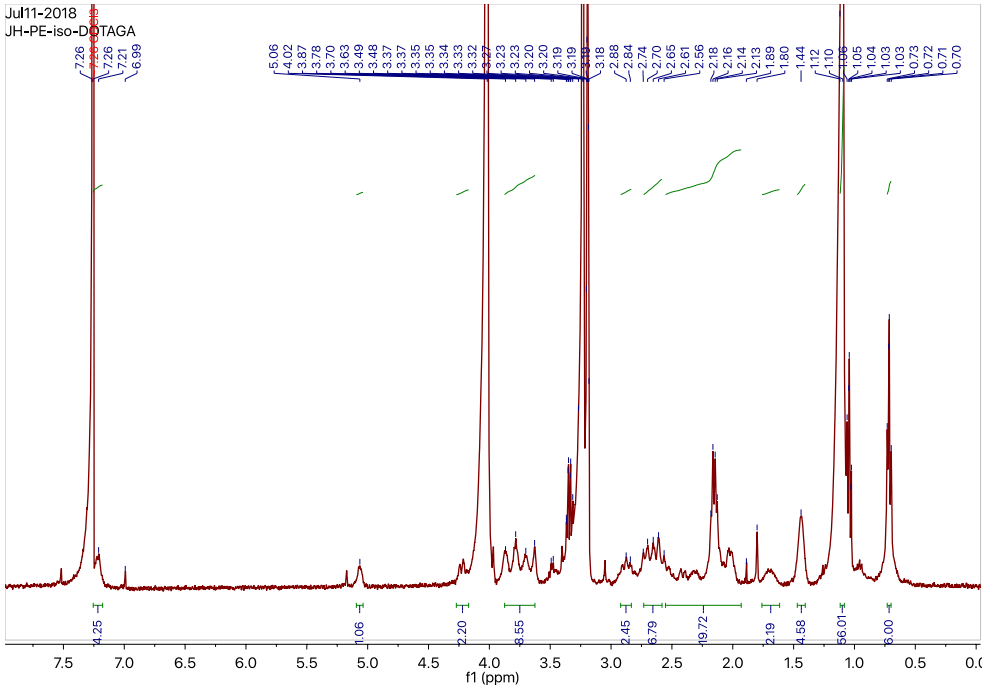


**Figure S17.** $^{1}$H NMR spectrum of PE-iso-DOTA-GA (**3**) in $CDCl_3$.

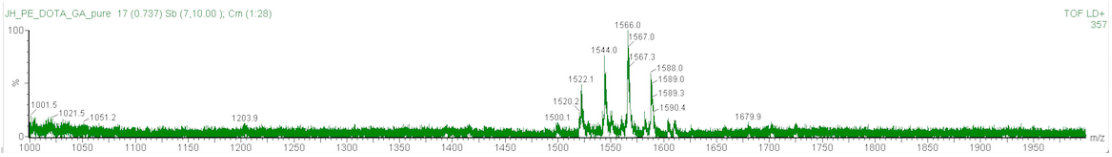


**Figure S18.** MALDI-TOF spectrum of PE-iso-DOTA-GA (**3**).

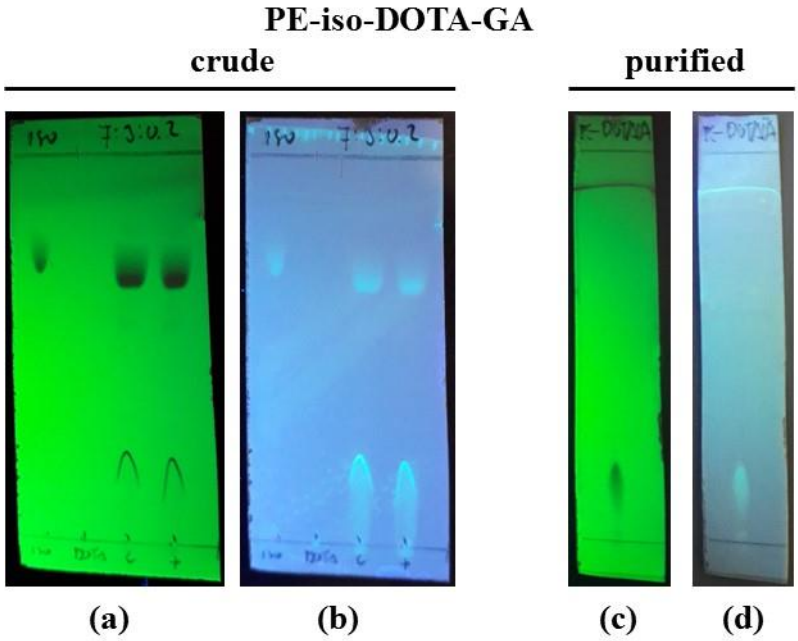


**Figure S19.** TLC plates of PE-iso-DOTA-GA reaction and purified lipid. (a), (c) and (e) under 254 nm UV lamp and, (b), (d) and (f) under 365 nm UV lamp and stained with a solution of 5% primuline. Mobile phase used for all plates composed of $CHCl_3$:MeOH:$H_2O$: a and b (7:3:0.2), c-f (5:5:0.2). PE = PE-$NH_2$ lipid, DOTA = DOTA-GA-$NH_2$, C = crude and, + = co-spot.

## Characterization of PE-PEG$_4$-TCO (4)

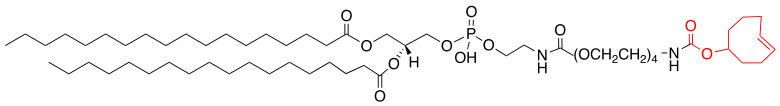

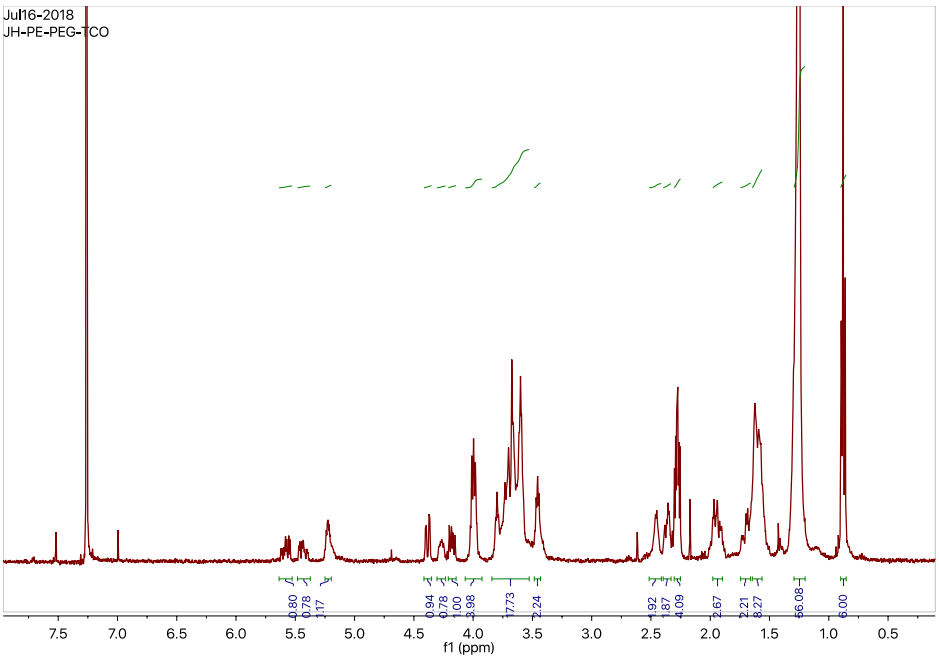


**Figure S20.** $^1$H NMR spectrum of PE-PEG$_4$-TCO (**4**) in $CDCl_3$.

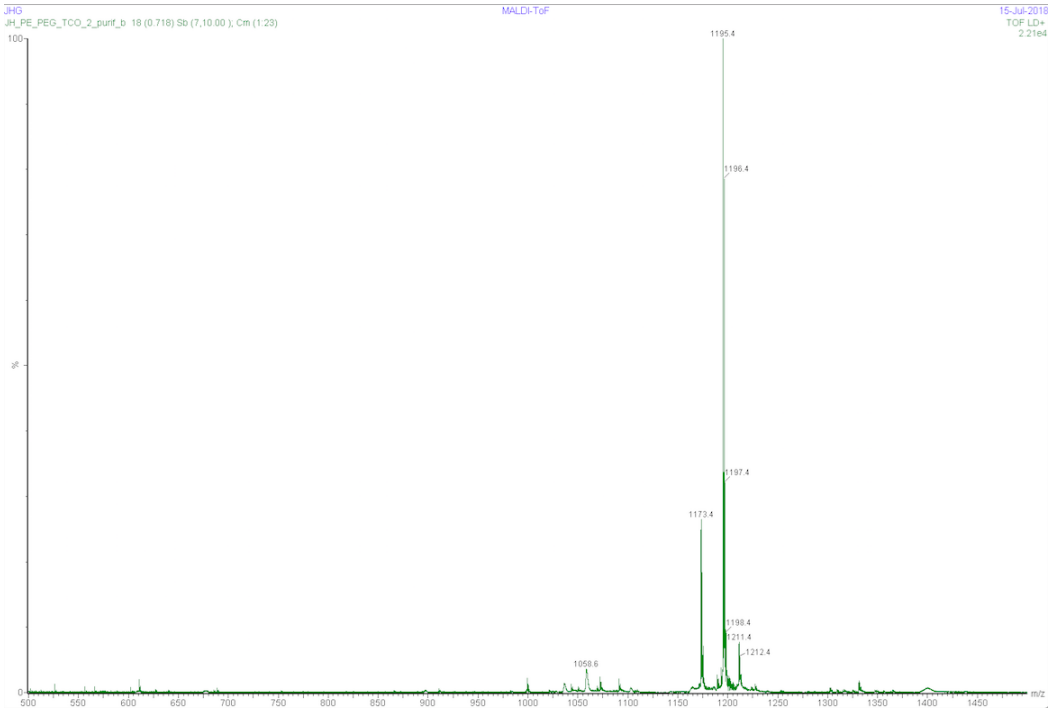


**Figure S21.** MALDI-TOF spectrum of PE-PEG$_4$-TCO (**4**) in $CDCl_3$.

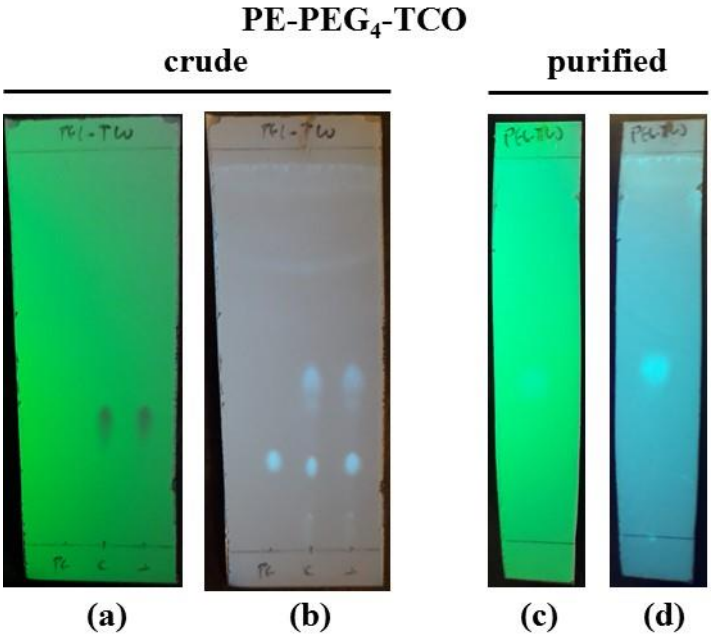


**Figure S22.** TLC plates of PE-PEG$_4$-TCO reaction and purified lipid. (a) and (c) under 254 nm UV lamp and, (b) and (d) under 365 nm UV lamp and stained with a solution of 5% primuline. Mobile phase: 8:2:0.2 ($CHCl_3$:MeOH:$H_2O$). PE = PE-$NH_2$ lipid, C = crude and, + = co-spot.

## Characterization of PE-TCO (7)

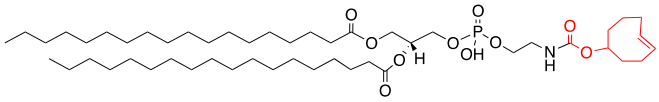

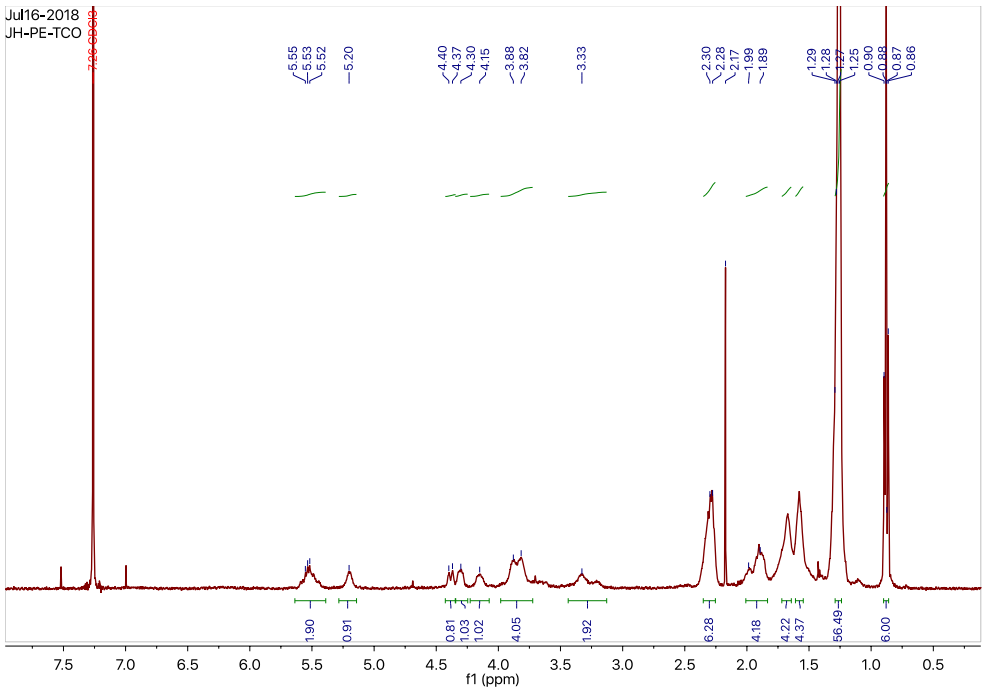


**Figure S23.** $^{1}$H NMR spectrum of PE-TCO (**7**) in $CDCl_3$.

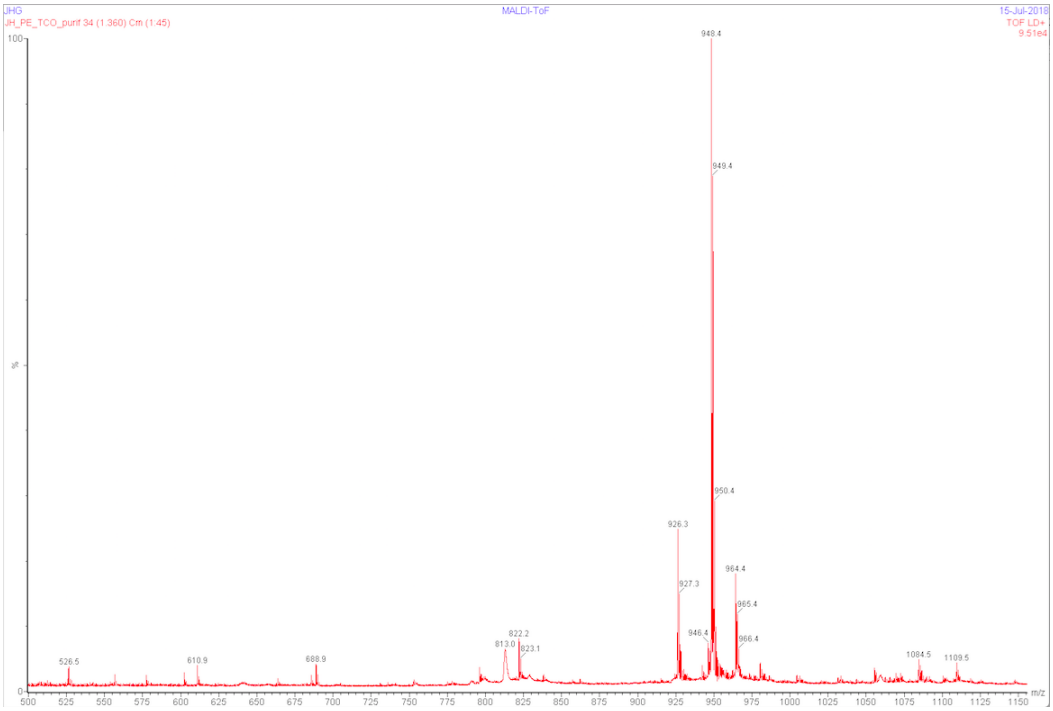


**Figure S24.** MALDI-TOF spectrum of PE-TCO (**7**) in $CDCl_3$.

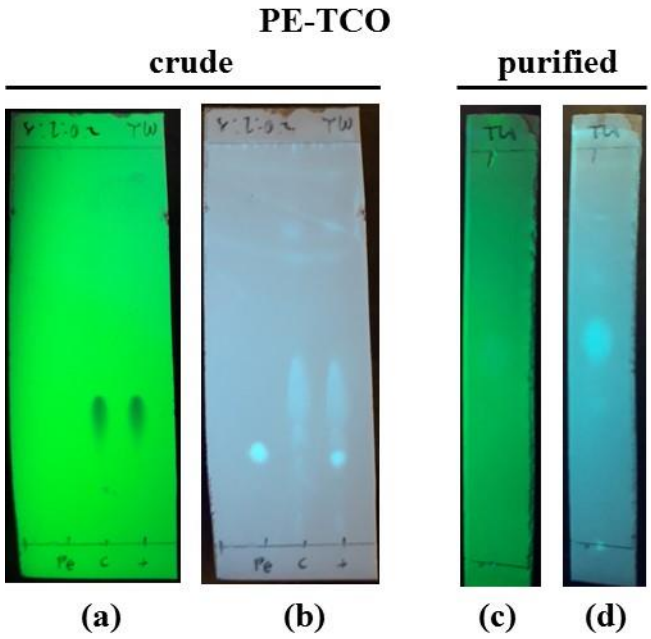


**Figure S25.** TLC plates of PE-TCO reaction and purified lipid. (a) and (c) under 254 nm UV lamp and, (b) and (d) under 365 nm UV lamp and stained with a solution of 5% primuline. Mobile phase used for both plates composed of $CHCl_3$:MeOH:$H_2O$: crude plate (8:2:0.2) and purified plate (7:3:0.2). PE = PE-$NH_2$ lipid, C = crude and, + = co-spot.

**Characterization of**

**3,3'-(((ethane-1,2-diylbis((carboxymethyl)azanediyl))bis(methylene))bis(4-hydroxy-3,1-phenylene))dipropionic acid (HBED-CC)**

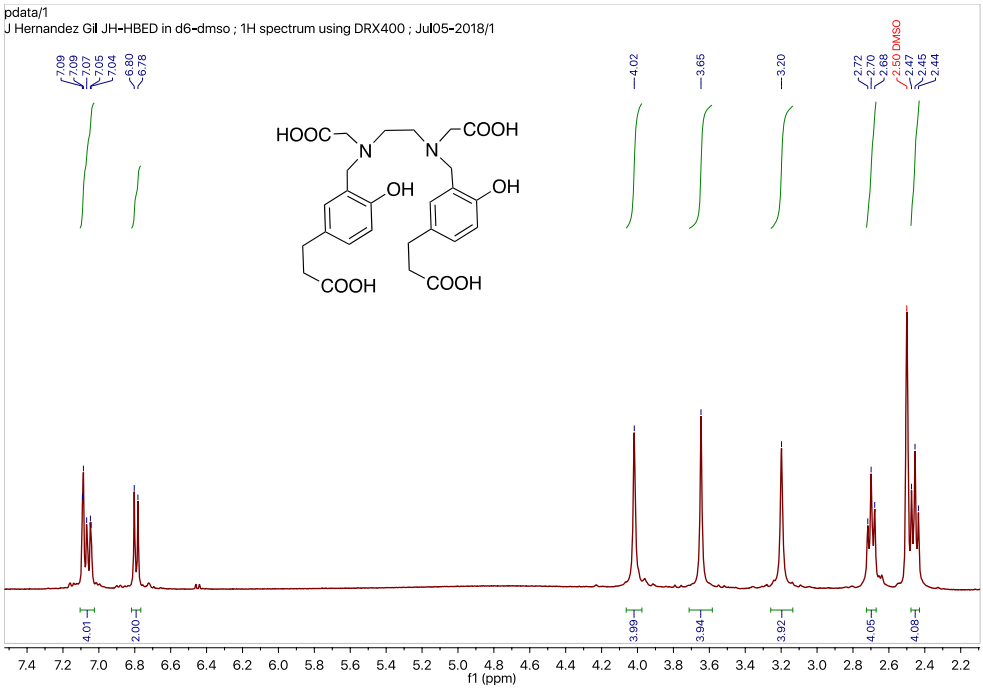


**Figure S26.** $^{1}$H NMR spectrum of HBED-CC in dmso-$d_6$.

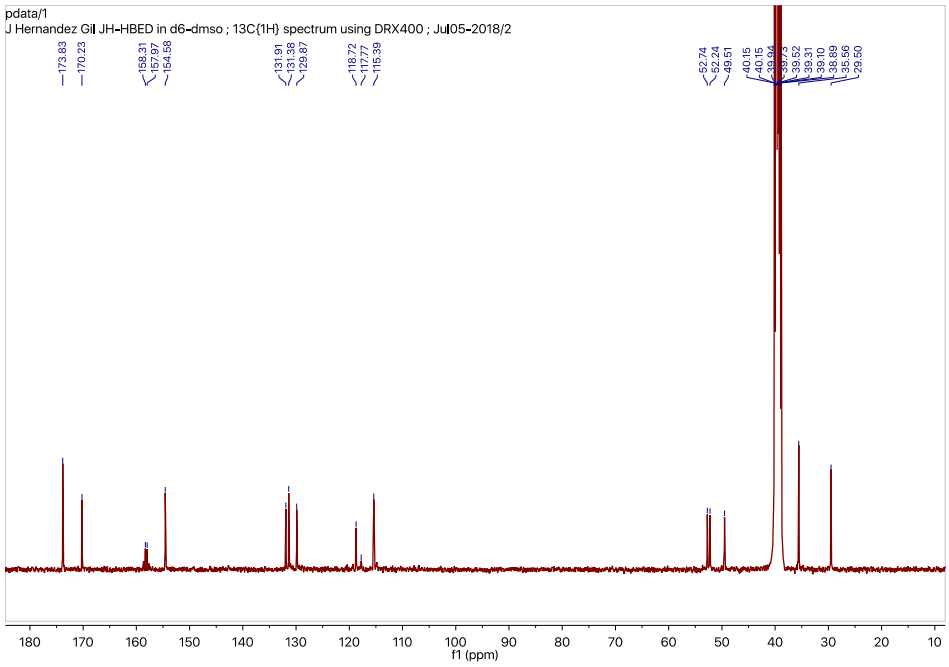


**Figure S27.** $^{13}$C NMR spectrum of HBED-CC in dmso-$d_6$.

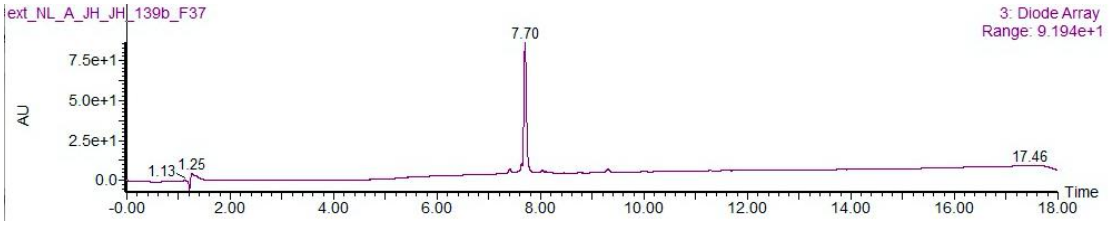


**Figure S28.** LC chromatogram of purified HBED-CC.

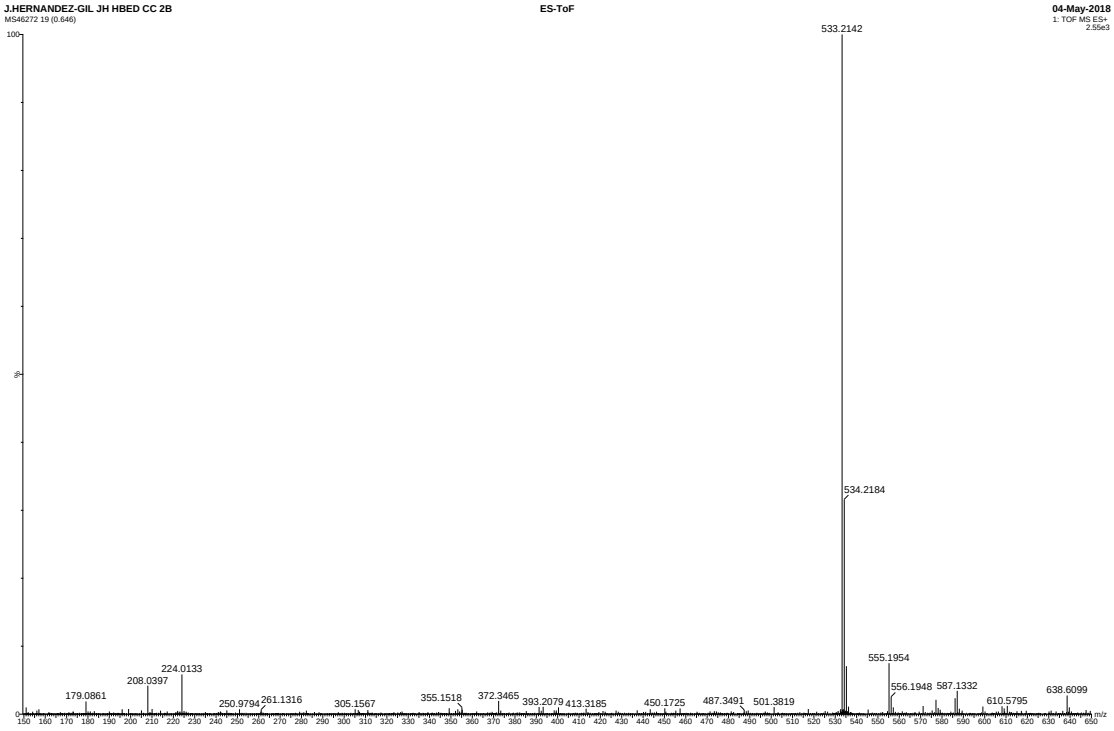


**Figure 29.** HR-ESI spectrum in positive mode of HBED-CC.

**Characterization of 3-(3-(((carboxymethyl)(2-((carboxymethyl)(2-hydroxy-5-(3-((4-(6-methyl-1,2,4,5-tetrazin-3-yl)benzyl)amino)-3-oxopropyl)benzyl)amino)ethyl)amino)methyl)-4-hydroxyphenyl)propanoic acid (HBED-CC-Tetrazine, 5)**

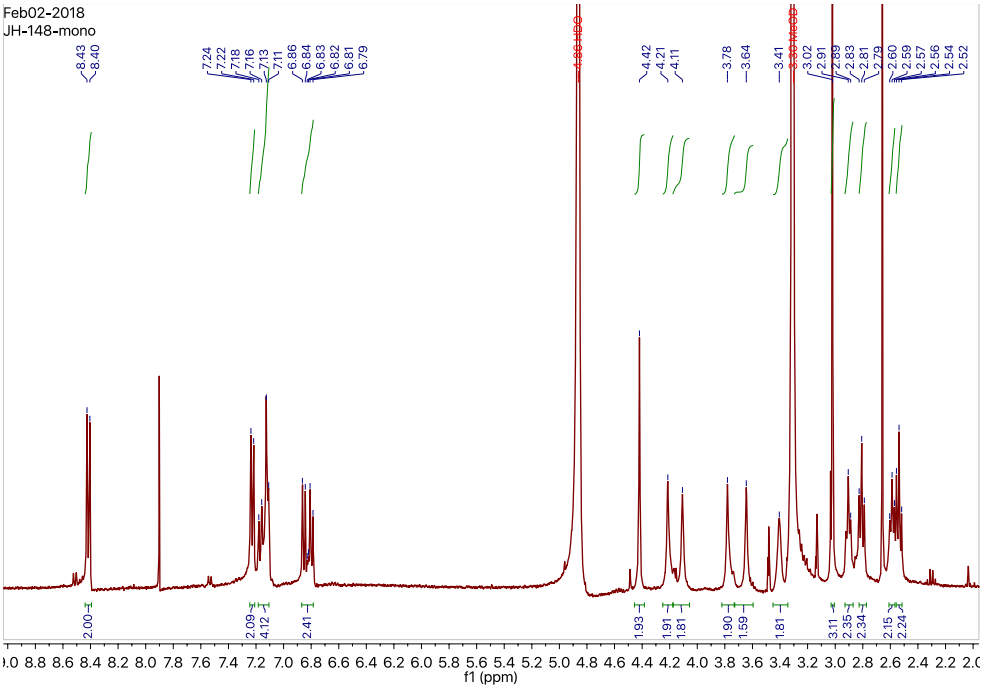


**Figure S30.** $^{1}$H NMR spectrum of HBED-CC-Tetrazine (**5**) in methanol-$d_4$.

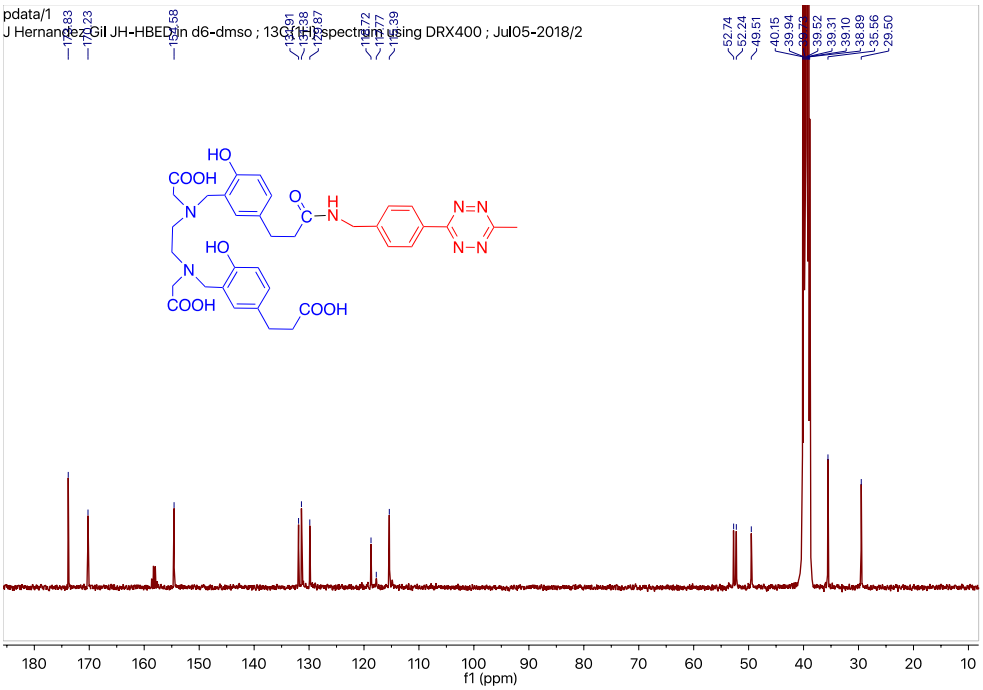


**Figure S31.** $^{13}$C NMR spectrum of HBED-CC-Tetrazine (**5**) in methanol-$d_4$.

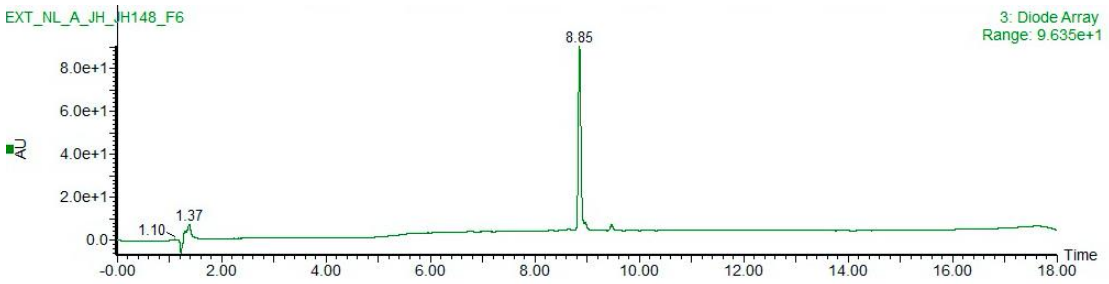


**Figure S32.** LC chromatogram of purified HBED-CC-Tetrazine (**5**).

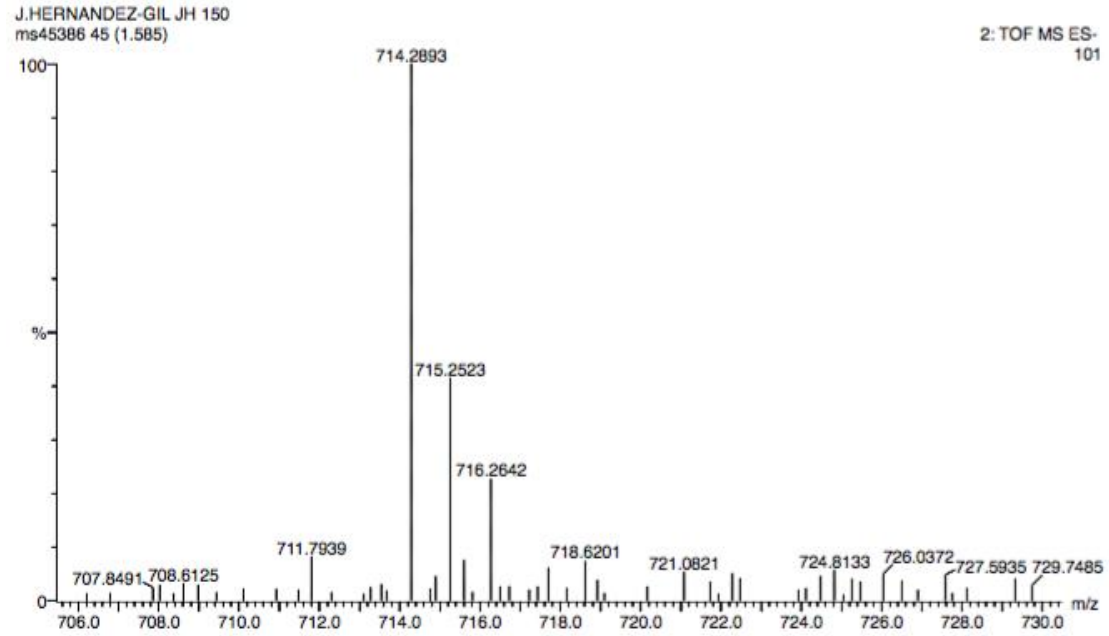


| | | | | | | |
|---|---|---|---|---|---|---|
| Minimum: | | | | -1.5 | | |
| Maximum: | | 5.0 | 10.0 | 50.0 | | |
| Mass | Calc. Mass | mDa | PPM | DBE | i-FIT | Formula |
| 714.2893 | 714.2888 | 0.5 | 0.7 | 20.5 | 3.5 | C36 H40 N7 O9 |

**Figure S33.** HR-ESI spectrum in negative mode of HBED-CC-Tetrazine (**5**).

**Characterization of *tert*-butyl (4-cyanobenzyl)carbamate.**

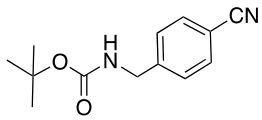


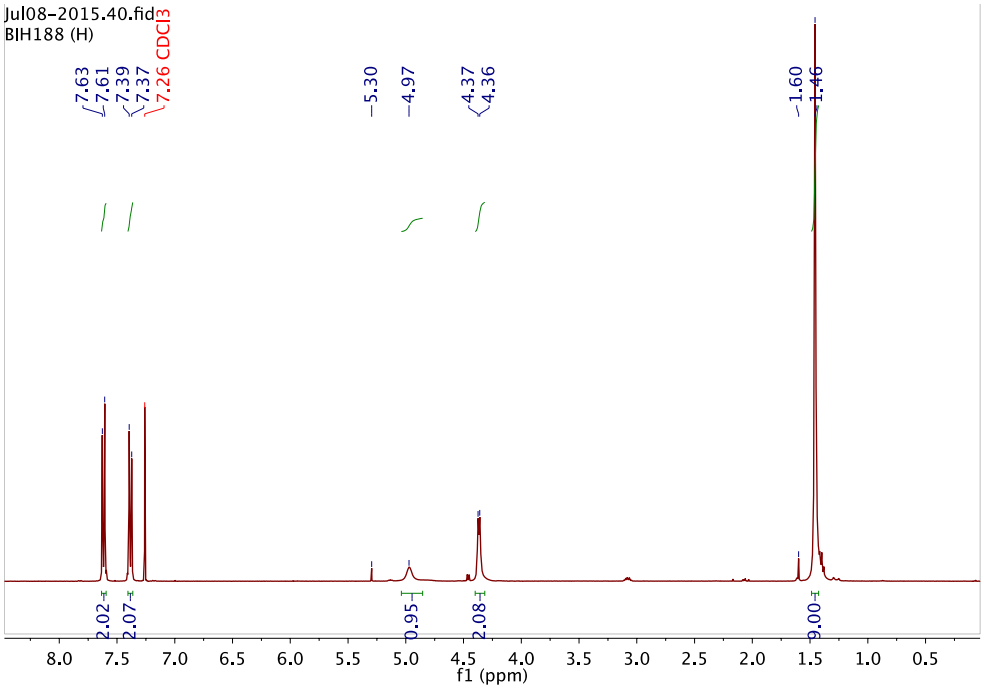


**Figure S34**. $^{1}$H NMR spectrum of *tert*-butyl (4-cyanobenzyl)carbamate in $CDCl_3$.

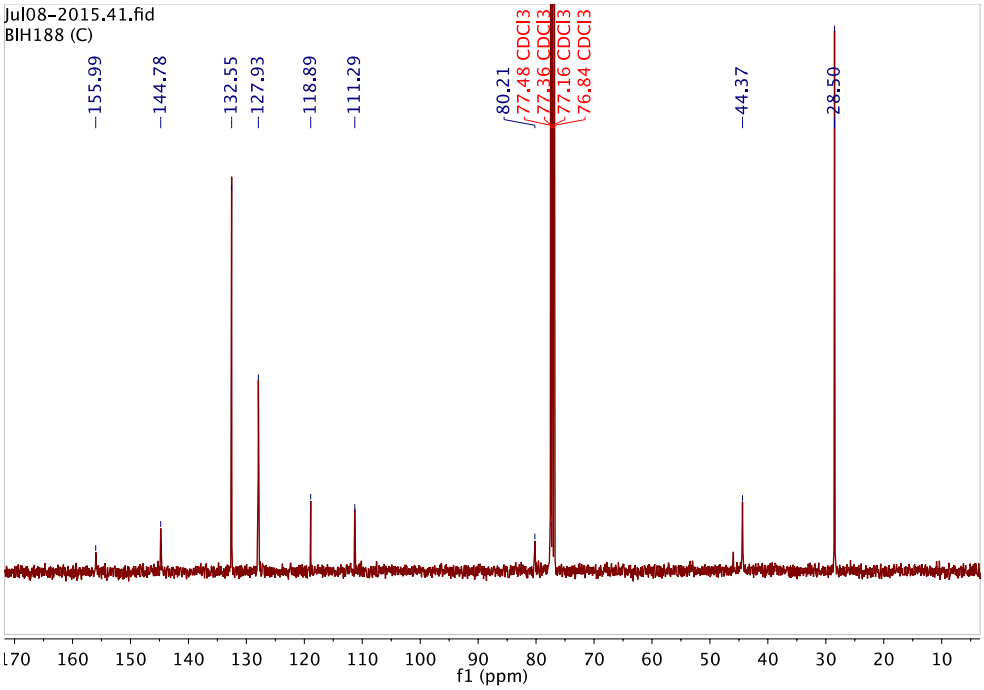


**Figure S35.** $^{13}$C NMR spectrum of *tert*-butyl (4-cyanobenzyl)carbamate in $CDCl_3$.

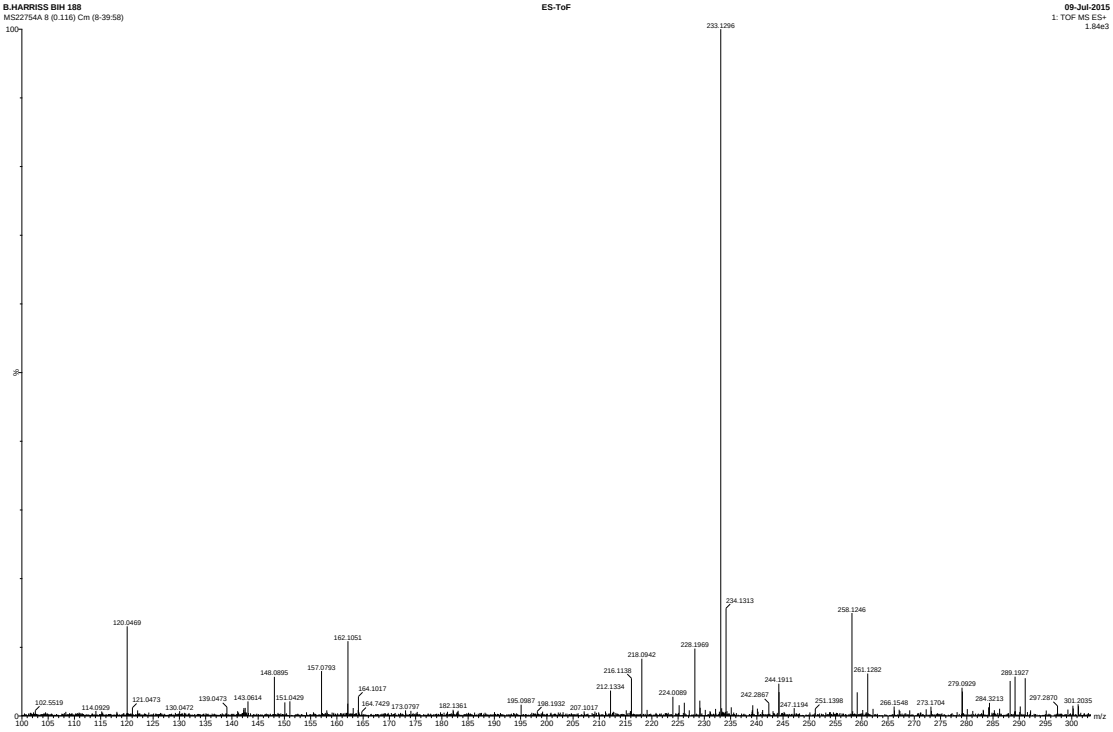


**Figure S36.** HR-ESI spectrum in positive mode of *tert*-butyl (4-cyanobenzyl)carbamate.

**Characterization of *tert*-butyl (4-(6-methyl-1,2,4,5-tetrazin-3-yl)benzyl)carbamate.**

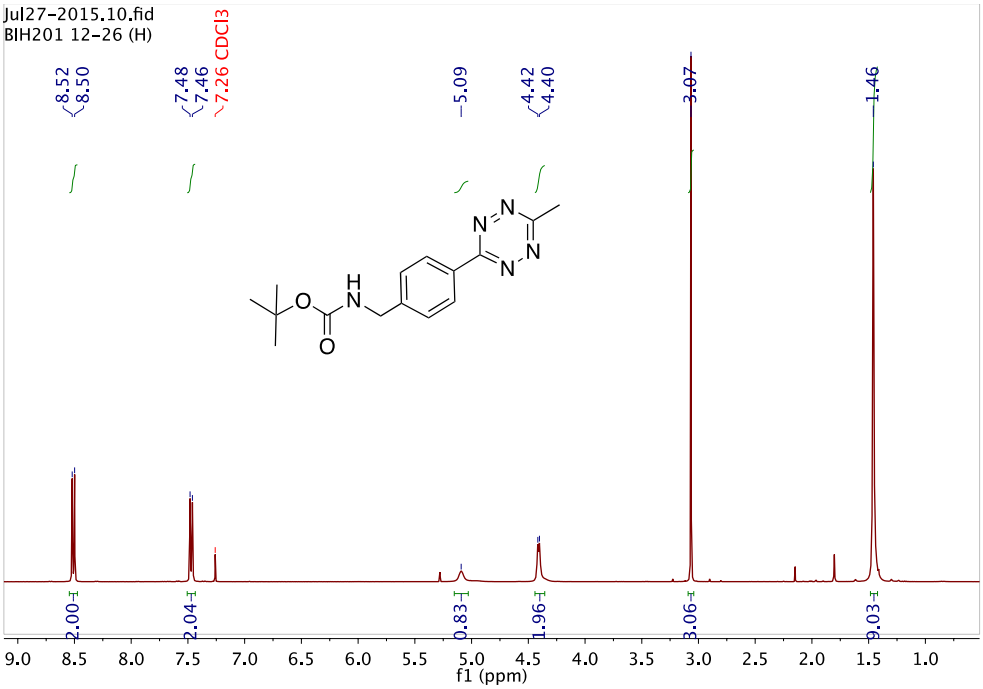


**Figure S37.** $^{1}$H NMR spectrum of *tert*-butyl (4-(6-methyl-1,2,4,5-tetrazin-3-yl)benzyl)carbamate in $CDCl_3$.

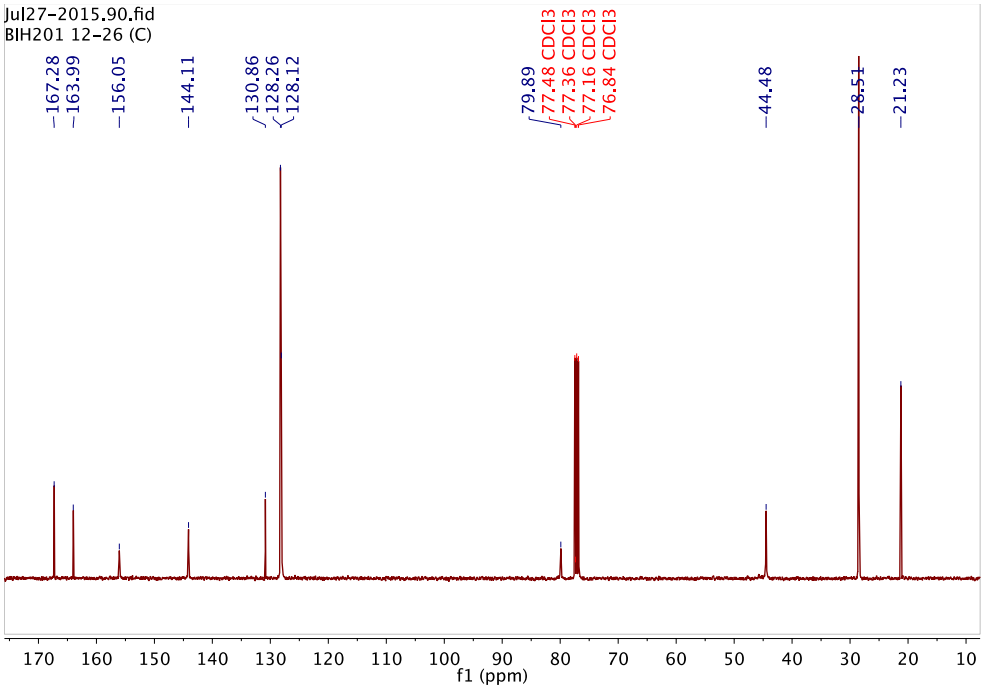


**Figure S38.** $^{13}$C NMR spectrum of *tert*-butyl (4-(6-methyl-1,2,4,5-tetrazin-3-yl)benzyl)carbamate in $CDCl_3$.

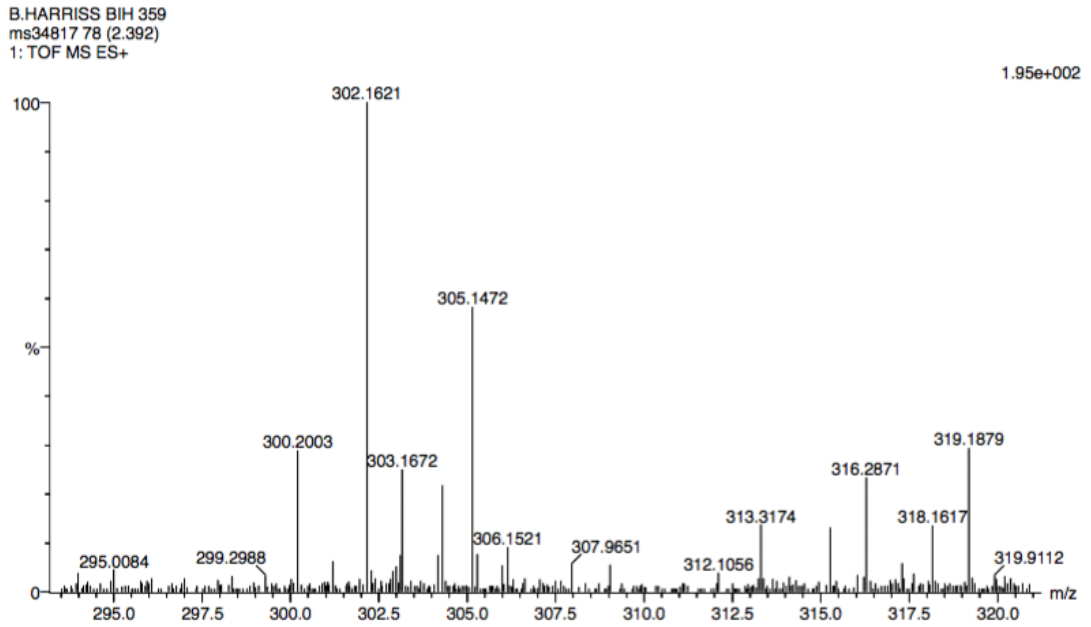


**Figure S39.** HR-ESI spectrum in positive mode of *tert*-butyl (4-(6-methyl-1,2,4,5-tetrazin-3-yl)benzyl)carbamate.

## Characterization of (4-(6-methyl-1,2,4,5-tetrazin-3-yl)phenyl)methanamine.

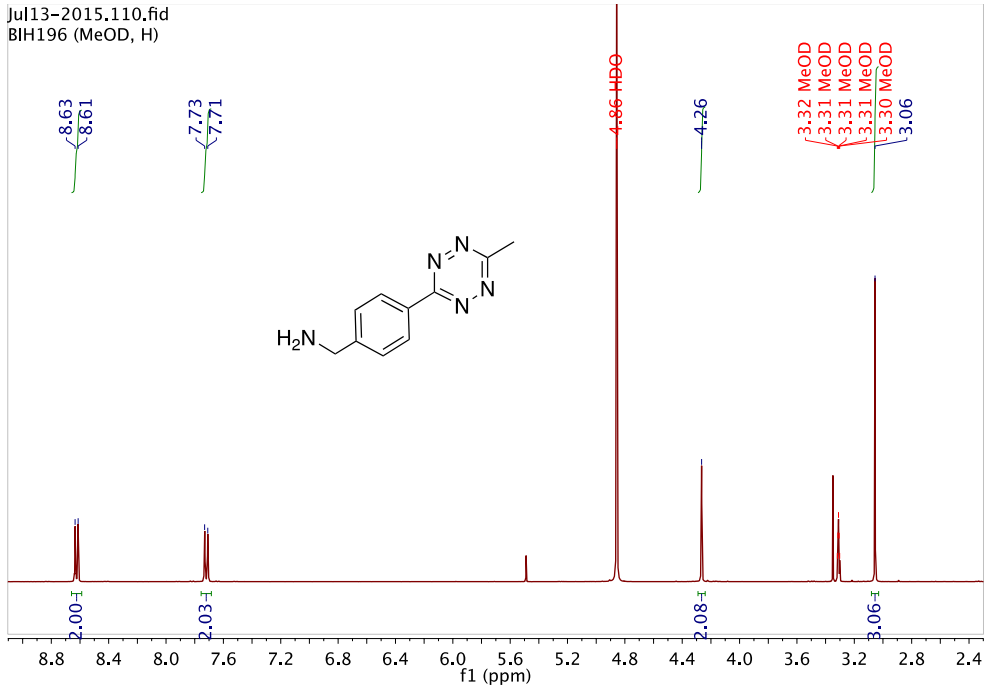


**Figure S40.** $^{1}$H NMR spectrum of (4-(6-methyl-1,2,4,5-tetrazin-3-yl)phenyl)methanamine in methanol-*d*$_4$.

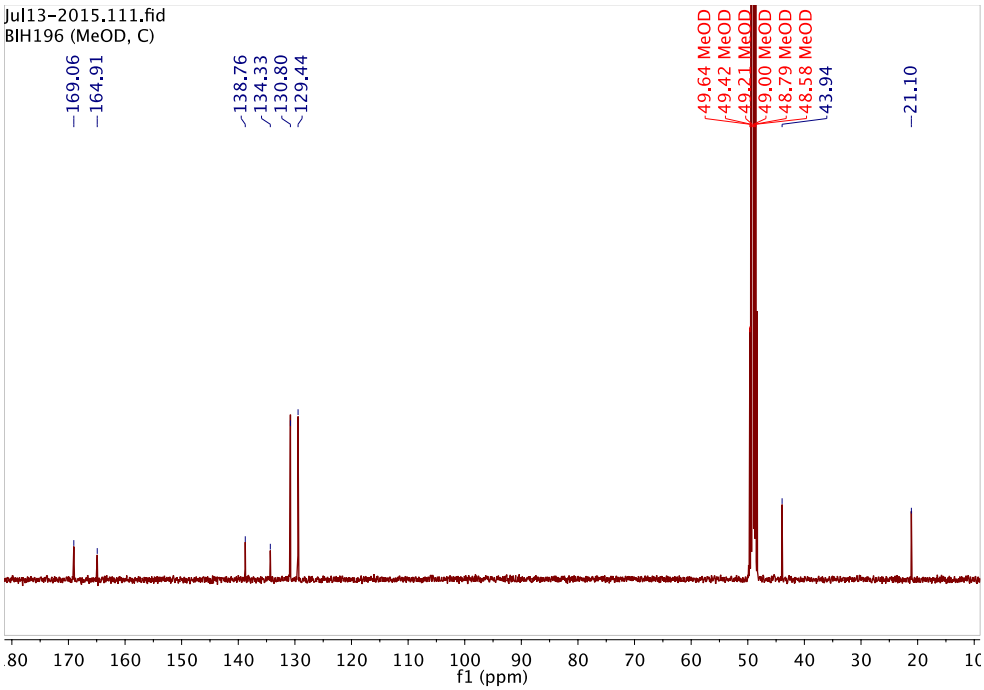


**Figure S41.** $^{13}$C NMR spectrum of (4-(6-methyl-1,2,4,5-tetrazin-3-yl)phenyl)methanamine in methanol-*d*$_4$.

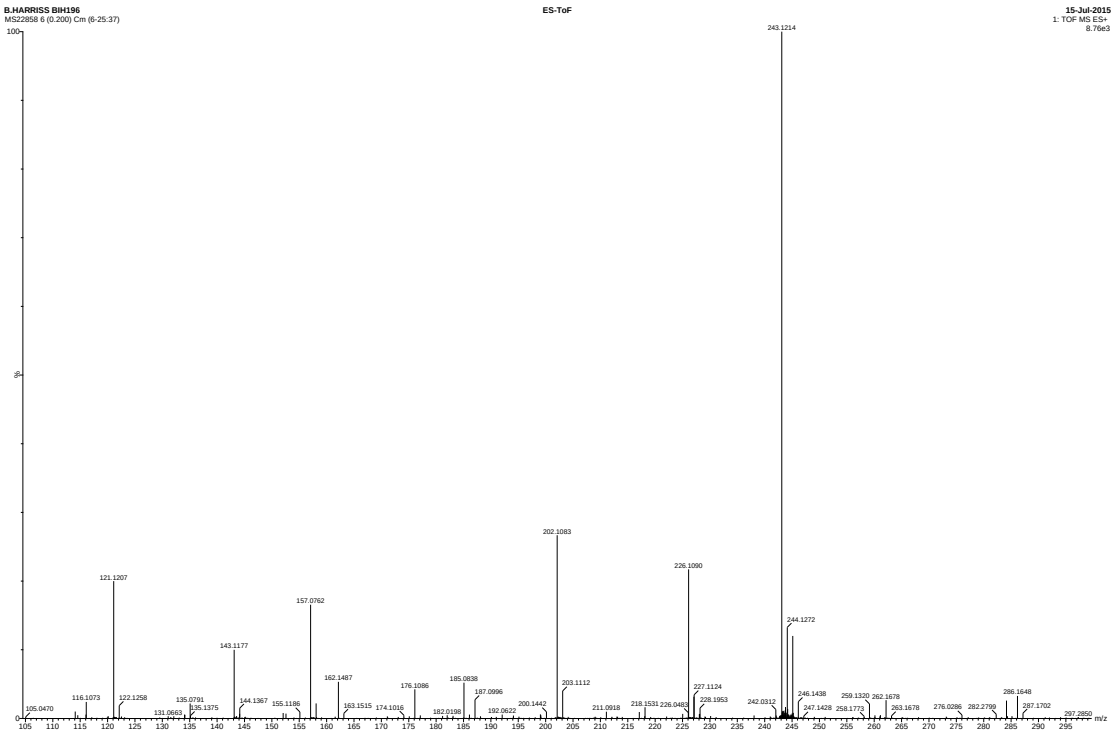


**Figure S42.** HR-ESI spectrum in positive mode of (4-(6-methyl-1,2,4,5-tetrazin-3-yl)phenyl)methanamine.

**Characterization of 5-((4-(6-methyl-1,2,4,5-tetrazin-3-yl)benzyl)amino)-5-oxopentanoic acid.**

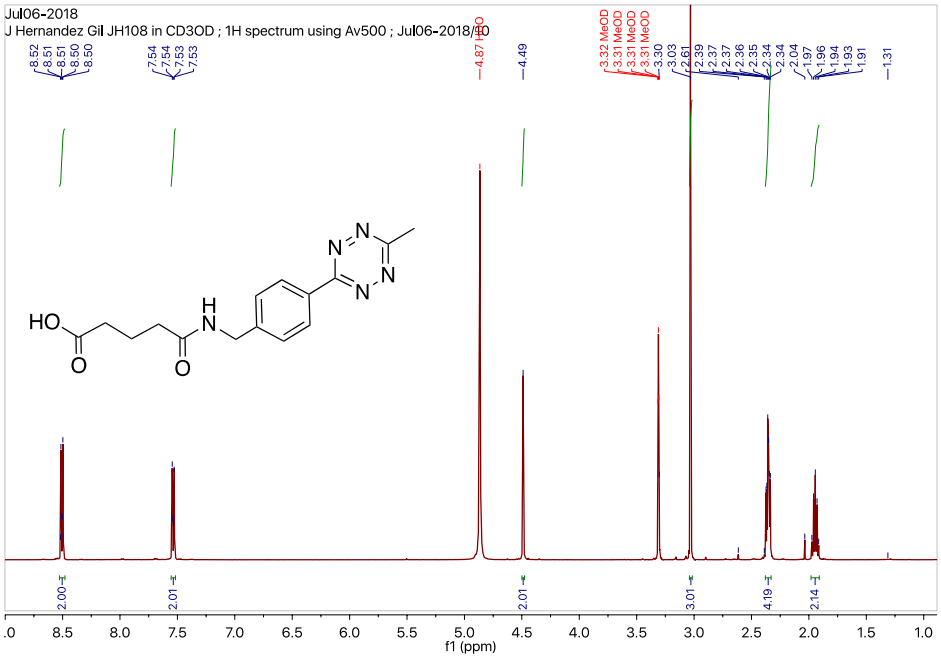


**Figure S43.** $^{1}$H NMR spectrum of 5-((4-(6-methyl-1,2,4,5-tetrazin-3-yl)benzyl)amino)-5-oxopentanoic acid in methanol-$d_4$.

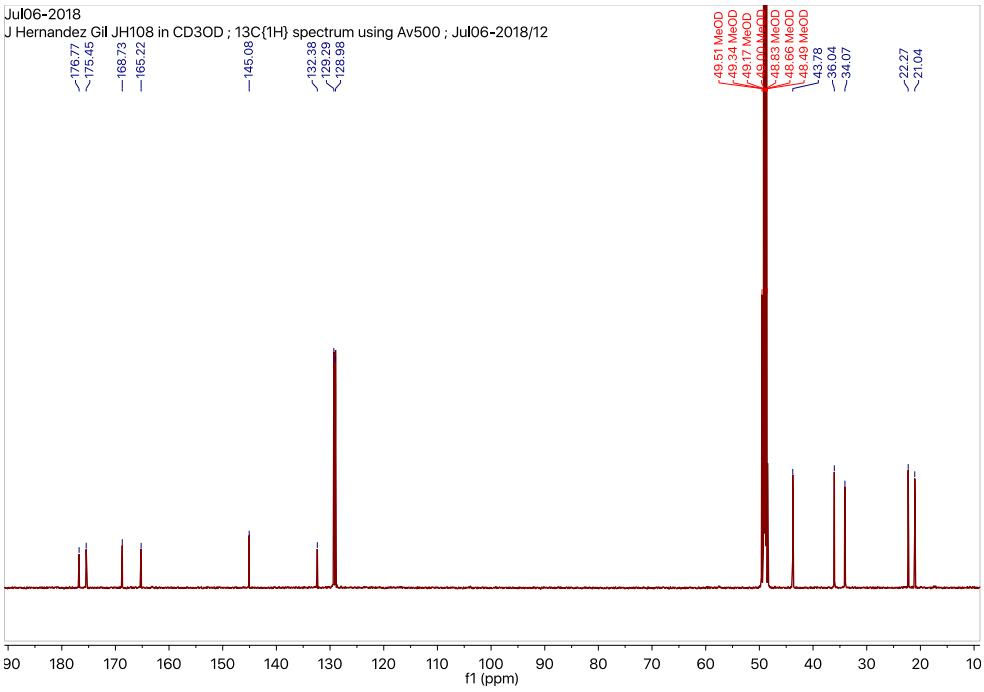


**Figure S44.** $^{13}$C NMR spectrum of 5-((4-(6-methyl-1,2,4,5-tetrazin-3-yl)benzyl)amino)-5-oxopentanoic acid in methanol-$d_4$.

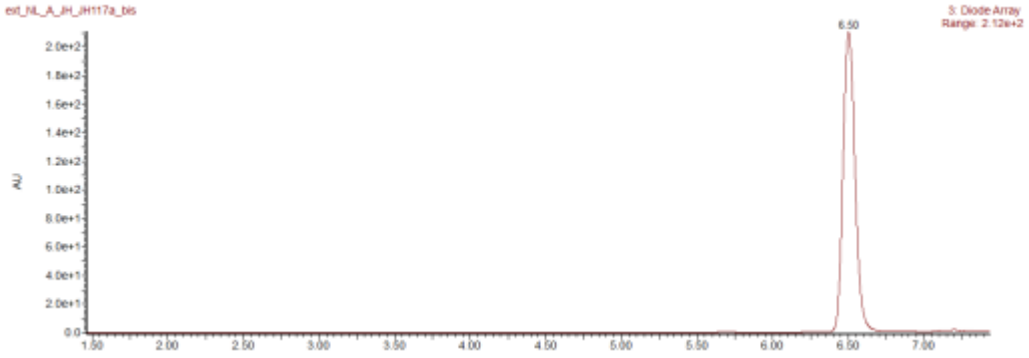


**Figure S45.** LC chromatogram of purified 5-((4-(6-methyl-1,2,4,5-tetrazin-3-yl)benzyl)amino)-5-oxopentanoic acid.

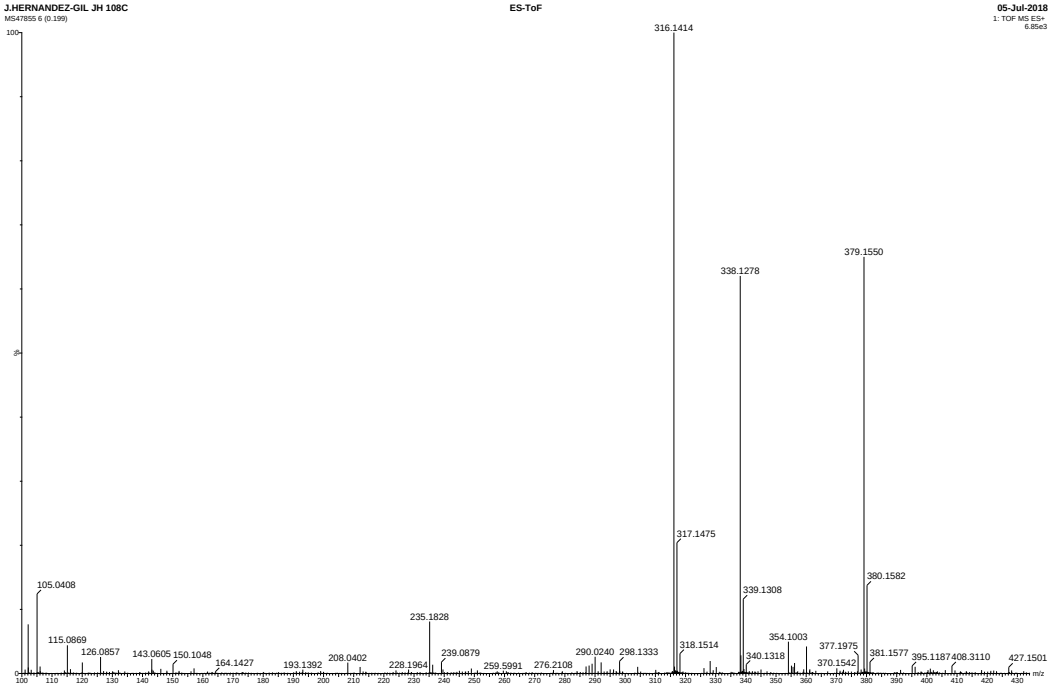


**Figure S46.** HR-ESI spectrum in negative mode of 5-((4-(6-methyl-1,2,4,5-tetrazin-3-yl)benzyl)amino)-5-oxopentanoic acid.

**Characterization of 2,2',2''-(10-(1-carboxy-4-((2-(5-((4-(6-methyl-1,2,4,5-tetrazin-3-yl)benzyl)amino)-5-oxopentanamido)ethyl)amino)-4-oxobutyl)-1,4,7,10-tetraazacyclododecane-1,4,7-triyl)triacetic acid (DOTA-GA-Tetrazine, 6)**

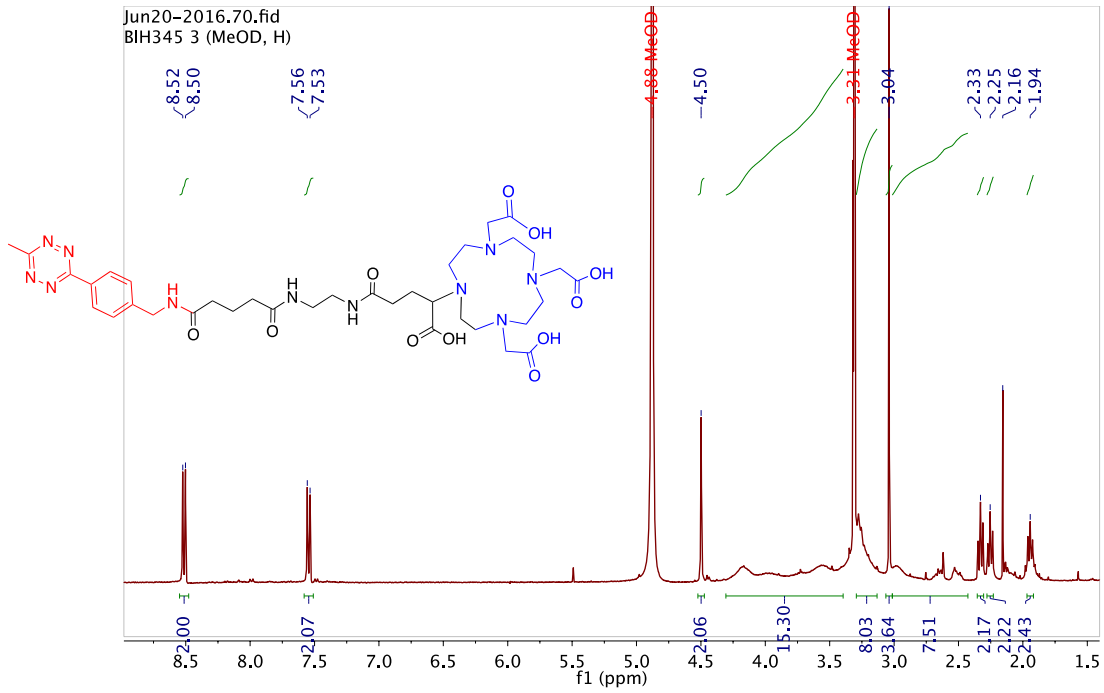


**Figure S47.** $^{1}$H NMR spectrum of DOTA-GA-Tetrazine (**6**) in methanol-$d_4$.

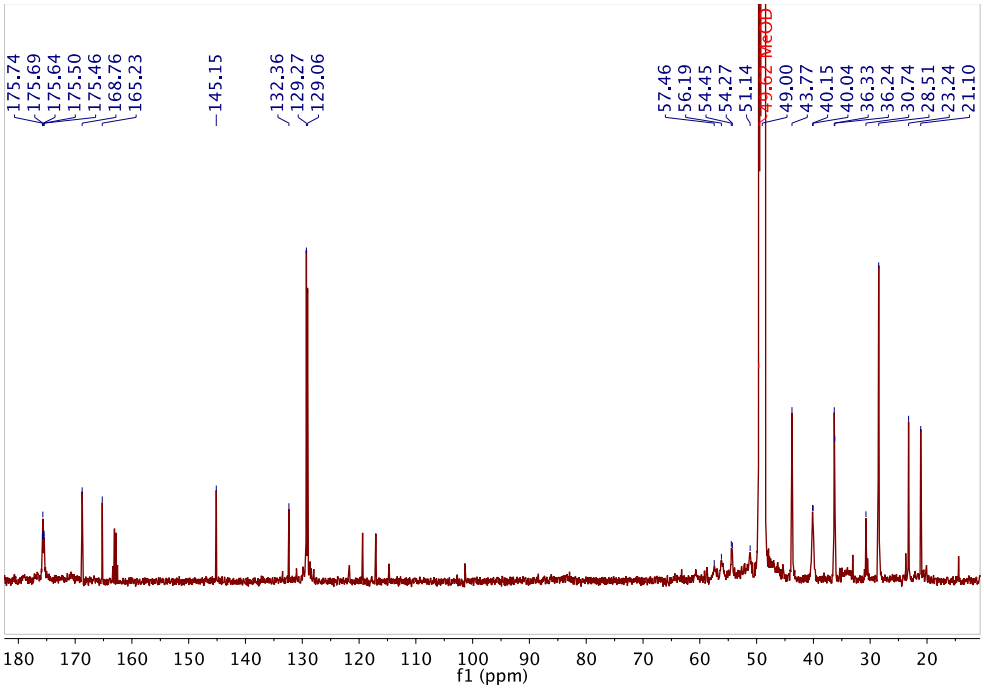


**Figure S48.** $^{13}$C NMR spectrum of DOTA-GA-Tetrazine (**6**) in methanol-$d_4$.

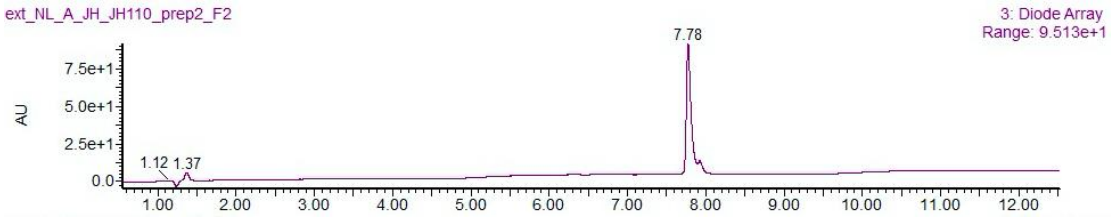


**Figure S49.** LC chromatogram of purified DOTA-GA-Tetrazine (**6**).

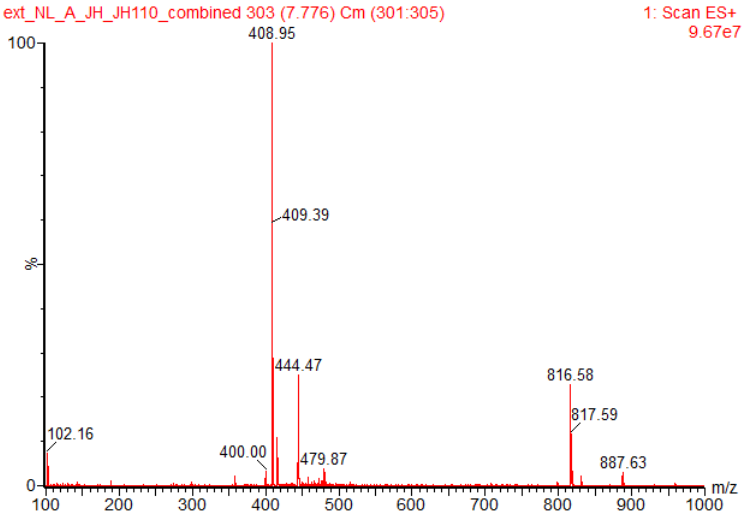


**Figure S50.** ESI spectrum in positive mode of DOTA-GA-Tetrazine (**6**).

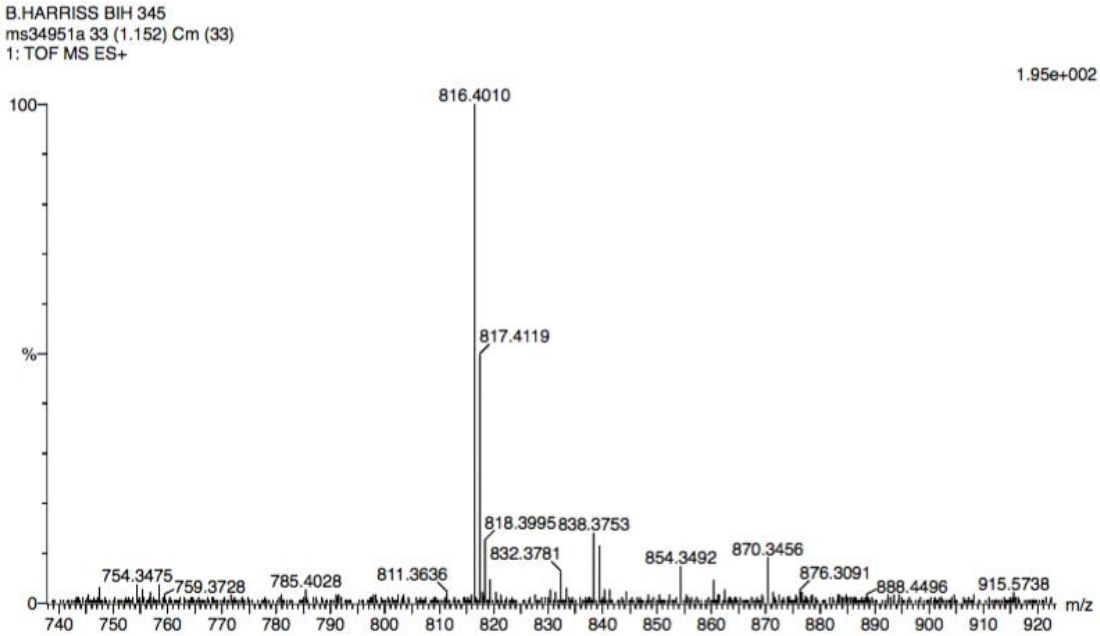


**Figure S51.** HR-ESI spectrum in positive mode of DOTA-GA-Tetrazine (**6**).